the plant journal

SEB SOCIETY FOR EXPERIMENTAL BIOLOGY

The Plant Journal (2025) **121,** e70085 doi: 10.1111/tpj.70085

INCREASED DNA METHYLATION 3 forms a potential chromatin remodelling complex with HAIRPLUS to regulate DNA methylation and trichome development in tomato

Tünde Nyikó[1], Péter Gyula[1,*], Szilvia Ráth[1], Anita Sós-Hegedűs[1], Tibor Csorba[1], Syed Hussam Abbas[1], Károly Bóka[2], Aladár Pettkó-Szandtner[3], Ágnes M. Móricz[4], Béla Péter Molnár[4], Anna Laura Erdei[4,5] and György Szittya[1,*]

[1]*Department of Plant Biotechnology, Hungarian University of Agriculture and Life Sciences, Gödöllő, Hungary,*
[2]*Department of Plant Anatomy, Eötvös Loránd University, Budapest, Hungary,*
[3]*Central Laboratories, Biological Research Centre, Szeged, Hungary,*
[4]*Plant Protection Institute, Centre for Agricultural Research, Eötvös Loránd Research Network, Budapest, Hungary, and*
[5]*Department of Plant Protection Biology, Swedish University of Agricultural Sciences, Alnarp, Sweden*

Received 14 August 2023; revised 13 February 2025; accepted 22 February 2025.
*For correspondence (e-mail szittya.gyorgy@uni-mate.hu and gyula.peter@uni-mate.hu).

SUMMARY

DNA methylation, a dynamic epigenetic mark influencing gene expression, is regulated by DNA demethylases that remove methylated cytosines at genomic regions marked by the INCREASED DNA METHYLATION (IDM) complex. In *Arabidopsis*, IDM3, a small α-crystalline domain-containing protein, stabilises the IDM complex. To investigate its role in tomato, we generated *slidm3* mutants using genome editing. These mutants displayed a 'hairy' phenotype with increased glandular trichomes, resembling the *hairplus* (*hap*) mutant. Affinity purification of SlIDM3-GFP associated proteins identified several chromatin remodelling factors, including HAP. Genome-wide DNA methylation analysis revealed sequence context dependent alterations in the *slidm3-1* plants, similar to the *hap* mutant. CHH methylation was predominantly increased, while CG methylation, particularly in intergenic regions, was decreased in both mutants. This imbalanced methylation suggests the presence of a 'methylstat' mechanism attempting to restore methylation levels at abnormally demethylated sites in the mutants. Comparative functional analysis of differentially methylated regions in the *slidm3-1* and *hap* mutants identified potential methylation-regulated genes that could be linked to the hairy phenotype. Our findings indicate that SlIDM3 may form a chromatin remodelling complex with HAP, epigenetically regulating trichome development.

Keywords: DNA methylation, DNA demethylation, Epigenomics, Chromatin remodelling, Gene expression regulation, Trichomes, Plant, Tomato.

INTRODUCTION

Epigenetics refers to heritable changes in gene expression that occur without modification of the underlying DNA sequence. Epigenetic regulation involves reversible post-translational modifications of histone proteins and the methylation of DNA which could alter the chromatin structure affecting DNA recombination, transposon silencing or regulation of gene expression (Law & Jacobsen, 2010; Matzke et al., 2015). Epigenetic marks could be inherited during DNA replication and cell division determining and maintaining cell type-specific gene expression patterns (Zhang et al., 2018). DNA methylation in plants can occur at cytosine residues both in symmetrical (CG or CHG) and non-symmetrical (CHH) contexts (where H can be an A, C, or T but not G) and is controlled by three classes of DNA methyltransferases (Zhang et al., 2018). Symmetric DNA methylation could be copied to the nascent DNA strand during DNA replication inheriting the methylation status of certain genomic regions to the daughter cells. On the other hand, asymmetric DNA methylation cannot be copied during replication but the methylation status could be transferred by a special group of 24-nt-long siRNAs (small interfering RNAs) that are produced by the concerted action of POLYMERASE IV (PolIV), RNA DEPENDENT RNA POLYMERASE 2 (RDR2), DICER-LIKE 3 (DCL3), and numerous other accessory proteins (Zhai et al., 2015). These siRNAs are cell-to-cell mobile and can travel systemically to distant tissues to induce *de novo* DNA methylation at siRNA-homologous sites (Tamiru et al., 2018). At the target sites, siRNAs are bound by

ARGONAUTE 4 (AGO4) type of proteins which can recognise homologous sequences in PolV-generated RNA transcripts. This interaction recruits DRM2 DNA methyltransferase that methylates nearby cytosine residues in the CHH context. This RNA dependent DNA methylation (RdDM) pathway is responsible for the silencing of transposable elements (TEs). If a TE resides in a promoter of a gene, the methylation status of this TE could affect the transcription of that gene (Galindo-González et al., 2018; Hollister & Gaut, 2009; Wang et al., 2013; Yamamuro et al., 2014).

Plants can also actively demethylate DNA via the action of DNA glycosylase-lyases, the so-called DEMETER-like DNA demethylases (DMLs) (Zhu, 2009). The active DNA demethylation by DMLs appear to be less sequence context dependent than the DNA methylation (Gehring et al., 2006; Gong et al., 2002; Hsieh et al., 2009; Ibarra et al., 2012; Penterman et al., 2007).

The mechanism of active DNA demethylation was extensively investigated in the model plant *Arabidopsis thaliana*. The main question was how certain methylated DNA regions are marked for demethylation while others are not. In the current model, the target selection of the DNA demethylases is defined by the INCREASED DNA METHYLATION (IDM) complex which marks the target sites for AtROS1 (also known as DML1). The *Arabidopsis* IDM complex contains two DNA binding proteins that recognise methylated cytosines, MBD7 (canonical Methyl-CpG-binding domain) and HDP2 (Harbinger transposon-derived DNA methyl-binding-protein) which ensure that the IDM complex is targeted to highly methylated regulatory sequences, where active DNA demethylation is required for gene expression (Lang et al., 2015; Nie et al., 2019). Two α-crystallin domain-containing proteins, IDM2 and IDM3 proteins hold the IDM complex together and connect the methylated DNA recognition components to the core enzyme, which is the IDM1 histone acetyltransferase. Furthermore, IDM2 and IDM3 also function as chaperone proteins to ensure IDM1 activity (Duan et al., 2017). The action of IDM1 create a permissive chromatin environment for recruitment and function of ROS1 and related DNA demethylases by specifically binding to chromatin sites that lack histone H3K4 di- or trimethylation and acetylating H3K18 and H3K23 (Qian et al., 2014; Zhao et al., 2014).

DNA methylation in the promoters of genes is known to inhibit gene transcription (Gehring & Henikoff, 2007; Zhang et al., 2010). Active removal of these inhibitory methylation marks during plant development and plant cell fate reprogramming could lead to an elevated gene expression (Liu & Lang, 2020; Zhang et al., 2022). DNA methylation also occurs in gene bodies of certain genes that are constitutively expressed ('housekeeping genes'), while inducible genes are usually depleted in gene body methylation and enriched in H2A.Z histone variant (Coleman-Derr & Zilberman, 2012; Zilberman et al., 2008). A recent study identified a third group of genes, the gene bodies of which are dynamically methylated and demethylated during development by the antagonistic action of DMLs and an unidentified, noncanonical *de novo* DNA methyltransferase that prefers CG context (Williams et al., 2023). Similar to several earlier studies, this study also could not find a direct correlation between gene body methylation and gene expression level. However, there was a correlation of gene body DNA methylation level heterogeneity and gene expression plasticity which was attributed to the action of DMLs.

The active DNA demethylation results in a hypomethylated state that could trigger *de novo* DNA methylation to restore the original methylation status. The global methylation level is measured by a methylstat mechanism (Lei et al., 2015; Williams et al., 2015). The basis of this mechanism is that the promoter of ROS1 DNA demethylase contains a TE that is target of ROS1 itself and also target of the RdDM pathway. For the proper expression of ROS1, this promoter region must be hypermethylated and should be bound by a group of SUVH and DnaJ-domain proteins that could maintain gene expression despite hypermethylation (Xiao et al., 2019). If this region is demethylated as the result of high ROS1 level, the expression of ROS1 is decreased. The hypomethylation triggers RdDM that restores the hypermethylated state of the methylstat region.

The tomato genome contains four putative *DML* genes encoding proteins with characteristic domains of functional DNA glycosylase-lyases (Liu et al., 2015; Mok et al., 2010). *SlDML1* and *SlDML2* are orthologous to the *Arabidopsis AtROS1* (*REPRESSOR OF SILENCING 1*) gene and *SlDML3* to *AtDME* (*DEMETER*), whereas *SlDML4* has no closely related *Arabidopsis* orthologue. All four *SlDML* genes are ubiquitously expressed in tomato plants, although *SlDML4* is expressed at a very low level in all organs (Liu et al., 2015). It was shown that the expression of *SlDML2* was increased during fruit ripening, and in line with this, in mutants lacking a functional *SlDML2* gene, fruit ripening was delayed (Lang et al., 2017). However, there is no information about the function of the other three DMLs in tomato.

A novel mutant named *hairplus* (*hap*) exhibiting a high Type I trichome density has been described in tomato (Fonseca et al., 2022). The *HAP* gene encodes for a SUVH3 histone lysine methyltransferase that binds methylated DNA and has lost its histone methyltransferase activity. It was shown that HAP promotes epigenetic modifications in the tomato genome and links epigenome remodelling with Type I trichome formation most likely through a novel genetic network (Fonseca et al., 2022). In this work, we show that a tomato homologue of the α-crystallin domain-containing protein IDM3 (SlIDM3) interacts

physically with HAP (SlSUVH3), SlIDM2, SlDNAJ1, and SlMBD5 and potentially forms a protein complex that causes DNA demethylation in the promoter and gene body regions of hundreds of protein coding genes. Consistent with this, our comparative DNA methylome analysis of *slidm3-1* and *hap* mutants revealed similar alterations in global DNA methylation patterns. Moreover, CRISPR/Cas9-generated *slidm3* mutants displayed the same increased trichome density (hairy phenotype) as *hap* mutants. Our findings suggest that SlIDM3, in conjunction with HAP, may epigenetically regulate the alternative splicing and expression of genes crucial for trichome development.

RESULTS

Generation of stable loss-of-function mutant alleles of *SlIDM3* using the CRISPR/Cas9 gene editing system

DNA methylation is a conserved epigenetic mark that plays important roles in development, gene expression regulation and genome stability. Cytosine methylation levels are dynamically regulated by DNA methylation and demethylation reactions. It was shown in *Arabidopsis* that IDM proteins enable DNA demethylases to prevent aberrant spreading of DNA methylation (Tang et al., 2016). IDM3 is an α-crystallin domain-containing protein that physically associates with other anti-silencing factors that prevent gene repression and hypermethylation at some genomic loci in *Arabidopsis* (Lang et al., 2015; Li et al., 2015). To study the molecular function of the tomato orthologue of *Arabidopsis* IDM3 (*SlIDM3*, Solyc04g082720), first we checked its expression in different tissues of tomato plants. We found that *SlIDM3* was ubiquitously expressed in all the tested tissues and was markedly induced during fruit ripening (Figure S1a). This observation suggested that SlIDM3, as a part of the hypothetical tomato IDM complex, may play a role in fruit ripening by marking the genomic sites for SlDML2-dependent DNA demethylation. The Arabidopsis IDM complex play a positive role in the regulation of DNA demethylation at dedicated sites, therefore, we expected that the lack of the *SlIDM3* would result in a fruit ripening phenotype similar to that of the *sldml2* mutant (delayed ripening).

To find out if *SlIDM3* plays a role in fruit ripening, we generated stable loss-of-function *slidm3* mutants using the CRISPR/Cas9 gene editing system. Two independent guide RNAs (gRNA) were designed to target the first exon of *SlIDM3* (Figure 1). We cloned the gRNAs along with Cas9 and Kan^R expression cassettes into a binary vector that was transformed into tomato plants (Moneymaker variety). Independent transformant lines (T0) were characterised by genotyping PCR and Sanger sequencing of the gRNA target regions (the primers used for the cloning and genotyping are listed in Table S1). Two independent homozygous T2 lines carrying single-nucleotide deletions causing frame-shift in the open reading frame of the *SlIDM3* gene

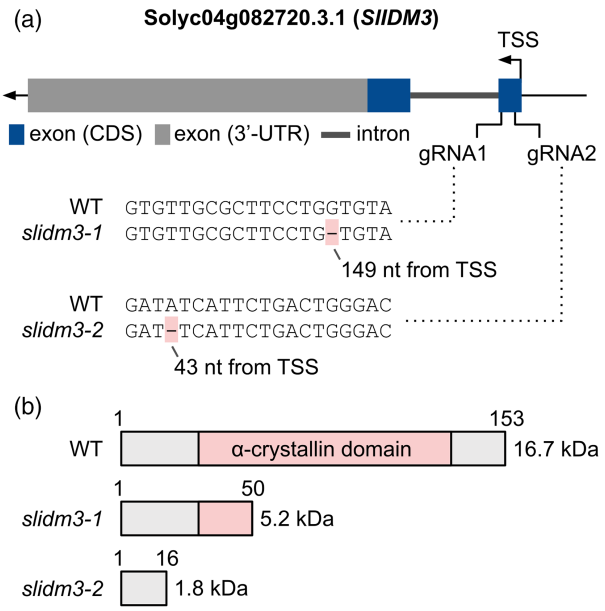

Figure 1. CRISPR/Cas9-based genome editing of *SlIDM3*.
(A) Structure of the *SlIDM3* gene showing the location of the two guide RNAs designed to target the first exon of the gene. The gene has two exons, the coding sequence (CDS) is separated by one intron. There is one long 3′ untranslated region (3′-UTR) and no annotated 5′-UTR. TSS: transcription start site. We obtained frame-shift mutants with both guides and we named them *slidm3-1* and *slidm3-2*.
(B) Both mutants express truncated versions of the small α-crystallin domain containing SlIDM3 protein. The number of amino acid residues and the theoretical molecular weights of the protein products are shown.

were selected and named *slidm3-1* (targeted by gRNA1), and *slidm3-2* (targeted by gRNA2) for further characterisation (Figure 1).

Contrary to our expectations, homozygous *slidm3-1* and *slidm3-2* plants showed no observable fruit ripening phenotype but exhibited a hairy phenotype in their vegetative and inflorescence stems when compared with wild-type (WT) plants (Figure 2a). The use of two independent lines created by two different guide RNAs makes the off-target effect unlikely as the explanation of the observed hairy phenotype.

In tomato, trichomes are multicellular and have been classified into eight different types, including both glandular (Type I, IV, VI and VII) and non-glandular (Type II, III, V and VIII) trichomes (Glas et al., 2012). Glandular trichomes produce specialised metabolites that are toxic or deterrent to pests, while non-glandular trichomes act as mechanical barriers that hinder pest movement along the plants (Simmons & Gurr, 2005). To investigate the trichome phenotype of the s*lidm3* plants in more detail, trichome identity and density of *slidm3-1* and WT plants were examined using optical and scanning electron microscopy. The *slidm3-1* and *slidm3-2* plants showed a higher density of Type I glandular trichomes than the WT plants on the vegetative and inflorescence stems (Figure 2b; Figure S2a).

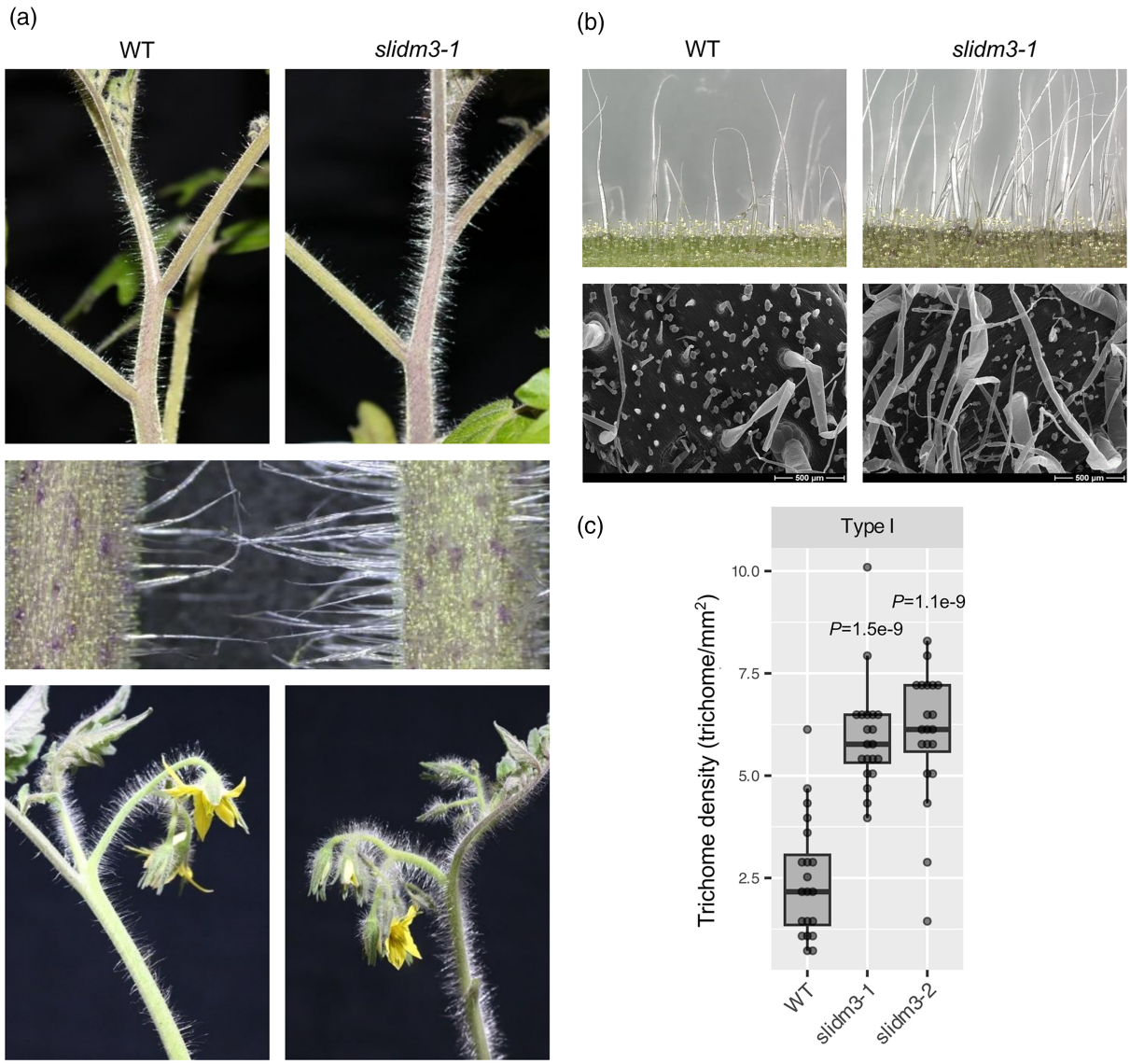

Figure 2. The *slidm3-1* mutant has increased glandular trichome density.
(A) The main vegetative stem (upper and middle panel) and the inflorescence stem (lower panel) of a wild-type (WT) Moneymaker plant and *slidm3-1* mutant plant with increased trichome density.
(B) Optical microscopic and scanning electron microscopic images of the stem of the wild-type and mutant plants.
(C) Density of Type I trichomes on WT, *slidm3-1* and *slidm3-2* mutant stems. Dunnett's test was performed to determine if there was a significant difference between the wild-type and the two mutants regarding trichome density. There was a significant difference between *slidm3-1* and WT (*P*-value = 1.5e-9) and also between *slidm3-2* and WT (*P*-value = 1.1e-9).

Additionally, we observed aberrant, branched Type I trichomes at different maturation stages on the leaves of *slidm3-1* mutant plants (Figure S2b,c), similar to the recently described *hairplus* (*hap*) mutant tomato plants (Figure S4 in Fonseca et al., 2022). Since tomato Type I glandular trichomes are the production sites of acyl sugars (Schuurink & Tissier, 2020), we checked the level of acyl sugars in the leaves and vegetative stems of WT and *slidm3-1* mutant plants. In accordance with the higher density of Type I trichomes, we observed higher acyl sugar levels in *slidm3-1* mutants compared with WT plants (Figure S3).

In summary, these results suggest that *SlIDM3* has a role to control Type I glandular trichome density in vegetative and reproductive organs in tomatoes.

Immunopurification and mass-spectrometric identification of SlIDM3 interacting proteins

IDM3 is a part of the IDM protein complex that participates in active DNA demethylation in *Arabidopsis* (Lang

Table 1 Mass-spectrometric analysis of proteins co-purifying with IDM3 in the stem and leaf

				Stem		Leaf	
Protein ID	Gene ID	Name	MW (kDa)	All/unique peptides	% Cov.	All/unique peptides	% Cov.
A0A3Q7GCP8	Solyc04g082720	*SlIDM3*	16.7	95/12	56.2	62/12	62.1
A0A3Q7EMV0	Solyc01g098810	*SlIDM2*	29.1	30/8	18.4	30/8	20.6
A0A3Q7ERD6	Solyc01g105780	*SlDNAJ1*	59.1	10/6	27.9	24/19	34.0
A0A3Q7IJC6	Solyc10g077070	*HAP*	78.4	66/21	42.7	112/48	64.3
A0A0S2GYF0	Solyc11g068740	*SlMBD5*	26.9	80/14	72.2	50/20	77.4

et al., 2015). To identify the components of the tomato IDM complex, we set out to purify the proteins associated with SlIDM3. We generated transgenic tomato plants expressing *SlIDM3-GFP* driven by the 35S promoter. The presence of the SlIDM3-GFP fusion protein in the transgenic lines was confirmed by Western blot analysis and confocal fluorescence microscopy. The fluorescent microscopy analysis revealed that the SlIDM3-GFP is mainly localised in the nucleus (Figure S4), consistent with its proposed role as an IDM complex subunit.

We purified SlIDM3-GFP and its interacting proteins from stem and leaf extracts using magnetic beads covered with anti-GFP antibodies. As a background control, the purification procedure was also carried out with samples from plants overexpressing GFP only. Tryptic peptides derived from the purified proteins were determined by mass spectrometry (Table 1; Table S2). We performed a differential expression analysis to identify significantly enriched proteins in the SlIDM3-GFP samples compared with the background samples. The resulting list contained orthologues of known *Arabidopsis* IDM3 interacting proteins such as SlIDM2 and SlSUVH3 (HAIRPLUS). The presence of DnaJ-domain proteins, SlMBD5 and PICKLE-homologues was also verified (Table 1). The full list of the identified proteins can be found in Table S2. To further validate our findings, the interactions of SlIDM3 with HAP/SlSUVH3, SlIDM2, SlMBD5 and SlDNAJ1 were confirmed in a co-immunoprecipitation experiment conducted in agroinfiltrated *Nicotiana benthamiana* leaves (Figure 3).

The presence of the HAP protein in the SlIDM3-interacting complex and the shared hairy phenotype of the *slidm3* and *hap* mutants suggested that both genes were involved in the epigenetic regulation of trichome development of tomato.

The *slidm3-1* mutation leads to alteration in the DNA methylome in a sequence context-dependent manner

In order to examine the possible role of SlIDM3 in epigenome remodelling, we selected the *slidm3-1* mutant line for further analysis. We performed a whole-genome bisulphite sequencing (WGBS) in three biological replicates to generate a single-base resolution map of DNA methylation from the vegetative stem of *slidm3-1* and WT plants because this tissue showed the strongest trichome phenotype. We obtained 9.5 M clean reads on average after adapter trimming and quality filtering (around 89% of the raw sequences) of which 81% mapped to the reference genome. The bisulphite conversion rate was uniformly 99.7%. The global methylation level of cytosine residues was 19.5%. Around 75% of the Cs in the CG context was methylated globally while the methylation percentage were 50 and 7.5 for the CHG and CHH context, respectively. The detailed sequencing statistics can be found in Table S3. These numbers indicated that the data were good quality and we proceeded with the identification of differentially methylated cytosines and regions between the mutant and the wild-type samples.

We found that the distribution of differentially methylated cytosines along the 12 tomato chromosomes was dependent on their sequence context. We observed that cytosines in the CHG and CHH sequence context (where H stands for a 'not G' nucleotide) were mostly hypermethylated in the *slidm3-1* mutant around the gene-rich regions (Figure 4a,b). Along the gene-rich chromosomal arms, the CG sites were also hypermethylated in the *slidm3-1* mutant compared with the wild-type (Figure 4a,b). However, we have detected mostly hypomethylated cytosines in the CG context in the pericentromeric regions.

Next, we identified the significantly differentially methylated regions (DMRs) in the *slidm3-1* mutant (Table S3). Our analysis identified 36 148 hyper-DMRs and 53 175 hypo-DMRs in *slidm3-1* plants. The genome-wide distribution of hyper-DMRs and hypo-DMRs was also sequence context-dependent (Figure 5). DNA hypomethylation in *slidm3-1* plants mostly occurred in the CG sequence context (8634 hyper-DMRs vs. 30 847 hypo-DMRs) while we observed more hypermethylation than hypomethylation in the CHH sequence context (19 995 hyper-DMRs vs. 10 822 hypo-DMRs). There were somewhat more hypomethylated than hypermethylated DMRs in the CHG context (7519 hyper-DMRs vs. 11 506 hypo-DMRs). Hypo-CHG DMRs were located mainly in intergenic regions, while hyper-CHG DMRs were mostly found in gene bodies

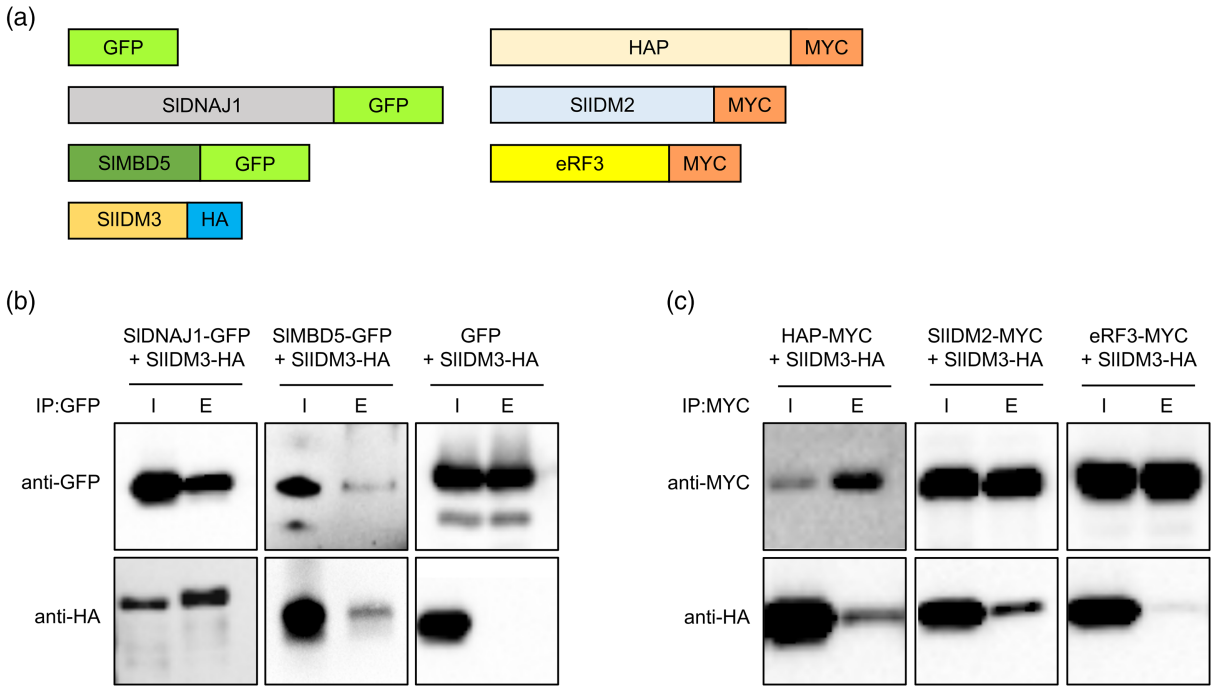

Figure 3. The SIIDM3 protein is associated with plant epigenetic regulators.
(A) Schematic, non-proportional representation of the constructs used in the co-immunoprecipitation experiments.
(B) *N. benthamiana* leaves were Agroinfiltrated with HA-tagged SIIDM3 (SIIDM3-HA) along with the GFP- or MYC-tagged partner. Three days after infiltration (3 dpi), proteins were extracted and affinity purification using magnetic beads covered with anti-GFP was carried out. Input (I) and elutes (E) were analysed by Western blot either with anti-HA antibody to test the presence of the prey (SIIDM3-HA) or anti-GFP to test the presence of the bait (the potential interactor).
(C) Same as B but the baits were tested with anti-MYC antibody. The GFP and the MYC-tagged eRF3 translation release factor (eRF3-MYC) were used as negative controls.

(Figure 5b). The overall number of hypermethylated DMRs was the highest in the CHH context and they mostly co-localised with gene-rich regions of the genome (Figure 5a), most notably with promoters, gene bodies, and other, unspecified regions (Figure 5b; Table S3). It must be noted that these regions quite often overlap with each other (i.e. a DMR can overlap with promoter and gene body, or promoter and repeats, etc).

In summary, we found a significant hypomethylation in the CG context in the gene depleted regions and hypermethylation mainly in the CHH context in the gene associated regions in the *slidm3-1* mutant compared with WT.

Gene expression changes in the *slidm3-1* mutant

DNA methylation is mainly associated with repression of transcription when it occurs in the promoter regions of genes (Zhang et al., 2018). Components of active DNA demethylation are also known as anti-silencing factors because of their function in preventing DNA hypermethylation and transcriptional gene silencing (Harris et al., 2018; Zhang et al., 2018). Since we observed DNA hypermethylation in the promoter region of protein coding genes of *slidm3-1* plants, we speculated that SIIDM3 may function to prevent transcriptional silencing of protein coding genes where DNA methylation could spread from nearby transposons to the promoters, as described earlier (Galindo-González et al., 2018; Hollister & Gaut, 2009; Wang et al., 2013; Yamamuro et al., 2014). Although we have found examples for this spreading (Figure S5), these were not associated with differential gene expression.

To gain insight into the role of SIIDM3 in the maintenance of gene expression, we determined the transcription profile in the vegetative stems of *slidm3-1* and WT plants in three biological replicates. We performed a differential gene expression analysis to get a list of the significantly differentially expressed genes (DEGs) between the WT and the mutant plants. We considered genes as differentially expressed when the *Q*-value was less than 0.05. Our analysis identified 169 upregulated and 268 downregulated genes in *slidm3-1* mutant plants (Figure 6a; Table S4) of which 12 and 16 encoded transcription factors (Table S4). There was no significant GO term enrichment among the upregulated genes but the term oxidation–reduction process (GO:0055114) and its parent terms were enriched in the list of the downregulated genes (Figure 6b; Figure S6, Table S4).

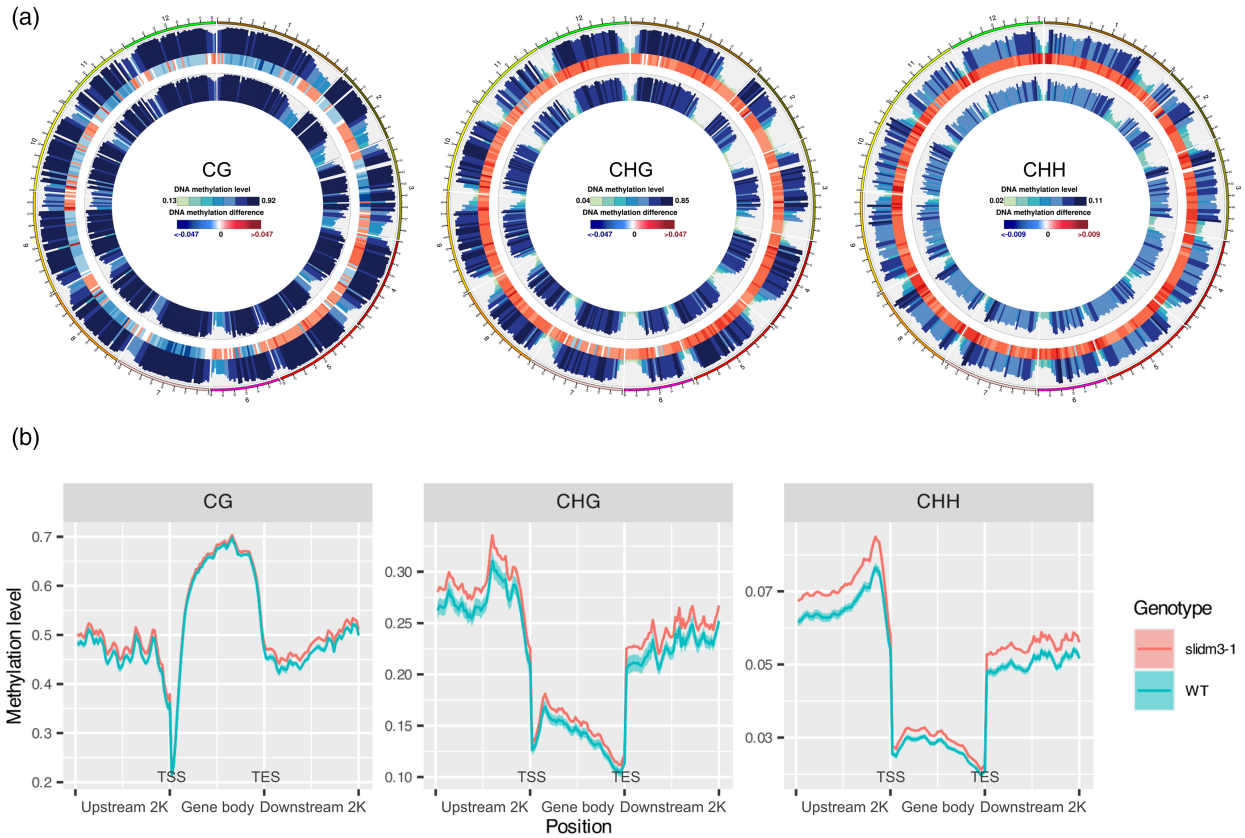

Figure 4. Genome wide cytosine methylation level is altered in the *slidm3-1* mutant.
(A) The 12 tomato chromosomes are shown as a circle. The circos plots represent (from outside to inside): 1. Methylation level along the genome in *slidm3-1*. 2. Methylation level difference between the *slidm3-1* and the WT. 3. Methylation level along the genome in the WT.
(B) An overview of methylation level distribution at up/downstream 2 kb and gene body in each sequence context (CG, CHG, CHH). The *x*-axis represents the functional genetic elements, the *y*-axis represents the methylation level. Each region was divided into 50 bins and methylation level was calculated in each bin. The lines represent the mean methylation level in the three biological replicates, while the coloured areas around the lines represent the standard error.

A number of different transcription factors involved especially in glandular trichome initiation and morphogenesis have been identified (Chalvin et al., 2020). Woolly (Wo), an HD-ZIP IV transcriptional factor, mainly regulating Type I trichome formation, was the first gene identified to control trichome development in tomato (Yang et al., 2011). A search for downstream factors uncovered a Cyclin B2 homologue in tomato (SlCYCB2) that was induced by Wo and participated in Wo-mediated Type I trichome development (Gao et al., 2017; Yang et al., 2011). This gene was recently renamed as multicellular trichome repressor 1 (MTR1; Wu et al., 2023). In the proposed model, Wo protein concentration is maintained by the opposing actions of MTR-mediated negative feedback regulation and self-reinforcement of expression. It was also demonstrated that Wo is a master transcriptional factor that specifies fates of multicellular trichomes via dosage-dependent mechanisms (Wu et al., 2023). Other transcription factors involved in glandular trichome development have also been characterised in tomato: The C2H2 zinc-finger protein HAIR (Chang et al., 2018) and the bHLH protein MYELOCYTOMATOSIS-RELATED 1 (SlMYC1) (Xu et al., 2018). The *HAIR* gene interacts with Wo and it is also essential for Type I trichome development (Chang et al., 2018). Another, R2R3-MYB type of transcription factor, the SlMIXTA-LIKE acts as a repressor of trichome formation and determines trichome patterning in leaves (Galdon-Armero et al., 2020). An earlier study showed that ectopic expression of SlMIXTA1 led to higher number of glandular and non-glandular trichomes in tomato; the plants produced more Type I trichomes, and RNAi plants had fewer Type I trichomes (Ewas et al., 2017, 2016).

Unfortunately, none of the differentially expressed transcription factors were known regulators of trichome development, although there were several members of the HD-ZIP, SBP, bHLH or Myb family of transcription factors known to regulate developmental patterns (Table S4). Furthermore, none of the transcripts of putative IDM complex members were changed at the transcriptional level.

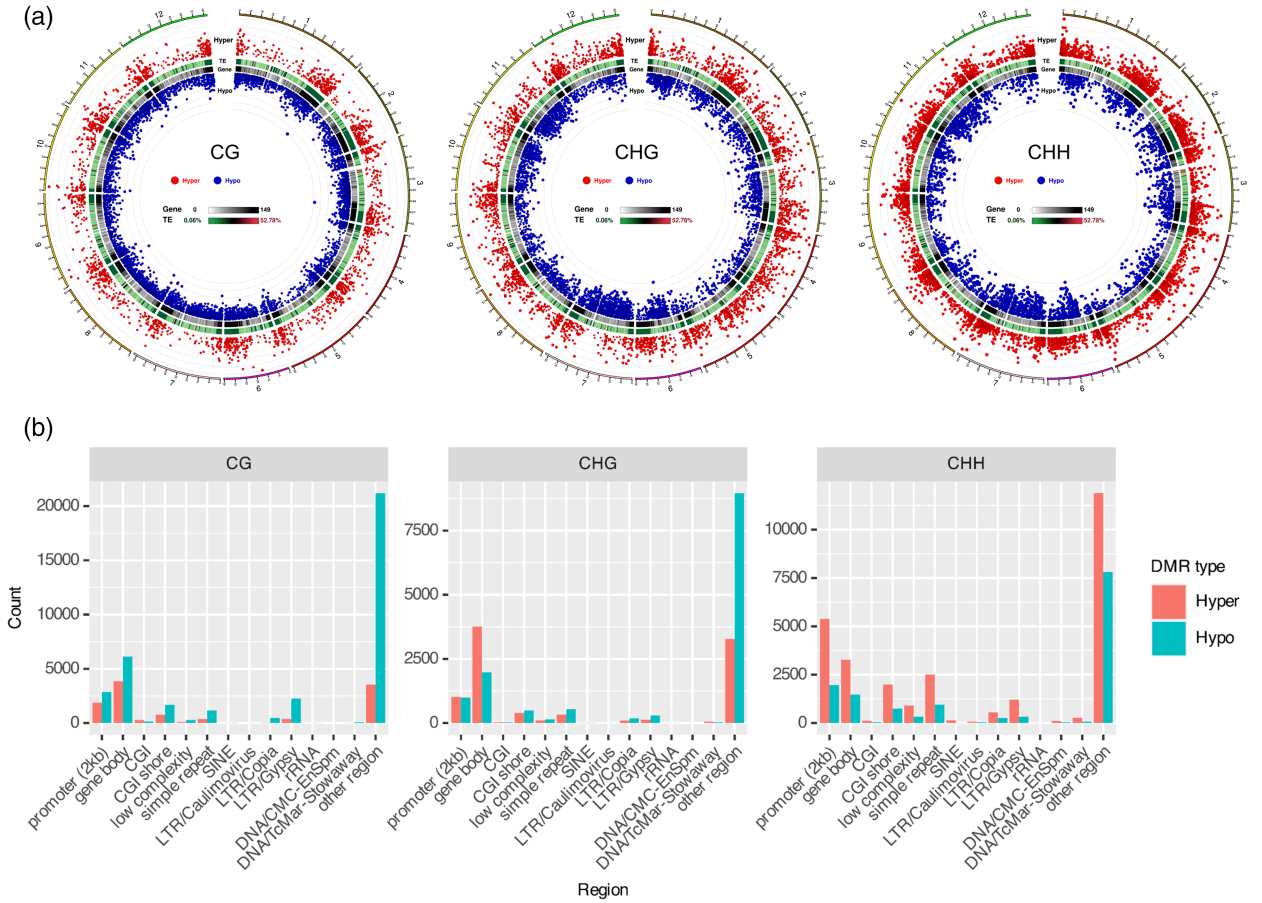

Figure 5. Differentially methylated regions in the *slidm3-1* mutant.
(A) The 12 tomato chromosomes are shown as a circle. The circos plots represent (from outside to inside): 1. Hyper-DMR statistical value by sequence context (CG, CHG, CHH). The higher and bigger the point, the larger the differences between two groups. 2. Transposable element (TE) density along the genome (less TE are located at the chromosome arms). 3. Gene density along the genome (more genes are located at the chromosome arms). 4. Hypo-DMR statistical value by sequence context.
(B) A summary of the DMRs by genomic annotations and by sequence context. Promoter: 2 kb upstream of gene feature; gene body: gene feature; CGI (CpG islands, CpG-rich regions); CGI shore: 2-kb-long regions that lie on both sides of a CGI; SINE: Short Interspersed Nuclear Element; LTR: various classes of Long Terminal Repeat type of retrotransposons; DNA: DNA transposons of various classes; other region: anything except the above categories, mostly intergenic regions.

Overlap between DEGs and DMRs

The higher number of CHH-hyper-DMRs in the promoter and gene body regions in the *slidm3-1* mutant suggested that DNA methylation/demethylation could affect the gene expression of the associated genes. To reveal such a possible regulatory effect, we investigated the overlap between the promoter and gene body localised DMRs and the DEGs. The analysis revealed that only a fraction of DEGs were associated with DMRs. And 68 up- and 95 downregulated DEGs of the 169 and 268 total up- and downregulated DEGs (40 and 35.5%, respectively) contained a DMR in their promoters, while 76 and 134 of them (45 and 50%, respectively) contained a DMR in their gene bodies. Only a small fraction of genes with promoter-associated DMRs (163 of the 10 244, 1.6%) or gene body DMRs (210 of the 11 362, 1.85%) were differentially expressed (Figure 6c; Figure S7). The most abundant overlapping sets between the DEGs and DMRs were the downregulated DEGs associated with gene body CG-hypomethylation only (18 genes) and promoter CHH-hypermethylation only (17 genes). The upregulated DEGs were associated either with promoter CHH-hyper- or hypomethylated DMRs only (9 and 6, respectively). There were many other combinations as well (Figure 6c).

Comparing the *slidm3-1* and *hap* transcriptome and methylome data

The interaction of SlIDM3 with HAP and the similar hairy phenotype of their mutants suggested that the two genes are involved in the same pathway that regulates DNA (de) methylation and trichome development. If this is true, one

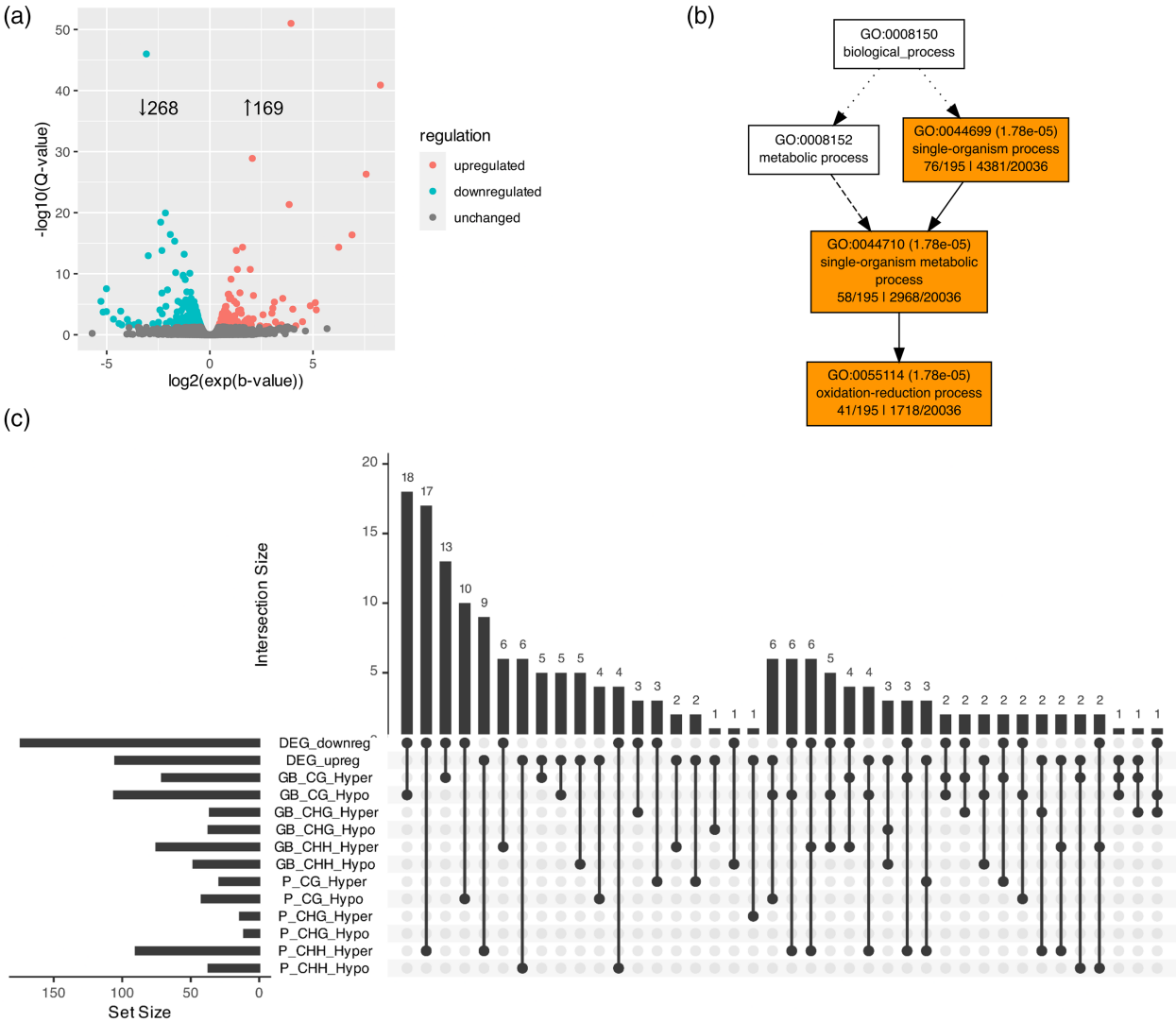

Figure 6. Gene expression changes in the *slidm3-1* mutant compared with wild-type.
(A) Volcano plot showing the distribution of the statistical significance values (*Q*-value or FDR corrected *P*-value on y-axis) of the differential expression of genes as a function of the magnitude of their change (estimated fold-change or *b* parameter in the model, x-axis). Genes were considered significantly differentially expressed if *Q*-value <0.05.
(B) Gene Ontology term enrichment analysis of the downregulated genes. Only the significantly enriched categories in the biological process supercategory are shown. The significantly enriched subcategories within the molecular function supercategory are shown in Figure S5. There were no significantly enriched categories in the list of upregulated genes.
(C) Intersections between the DEGs and gene body or promoter-associated DMRs. DMRs without associated DEGs or DEGs without DMRs in their promoters or gene bodies are not shown. These intersections are shown in Figure S7.

would speculate that the lack of either of them would result in a similar pattern of DNA methylation change and consequently a transcriptome change as well. Since the transcriptome and methylome data from the *hap* mutant is publicly available, we downloaded and analysed them in the same way as we analysed our *slidm3-1* dataset. Our transcriptome analysis resulted in 428 downregulated and 251 upregulated genes, whereas in the *hap* paper (Fonseca et al., 2022) the authors identified 82 downregulated and 8 upregulated genes in the *hap* mutant. The reason for the difference could be that we used different softwares and filtering rules. There were many transcription factor genes among the DEGs but they differed from the ones found in the *slidm3-1* mutant (Table S4d,i). When we compared the *hap* DEGs with the *slidm3-1* DEGs, we found only a moderate overlap: 44 genes were commonly downregulated and five genes were commonly upregulated in the two mutants with no transcription factor genes, while five genes were regulated oppositely (Figure 7a; Table S4i). To determine whether the observed overlaps occurred by chance, we

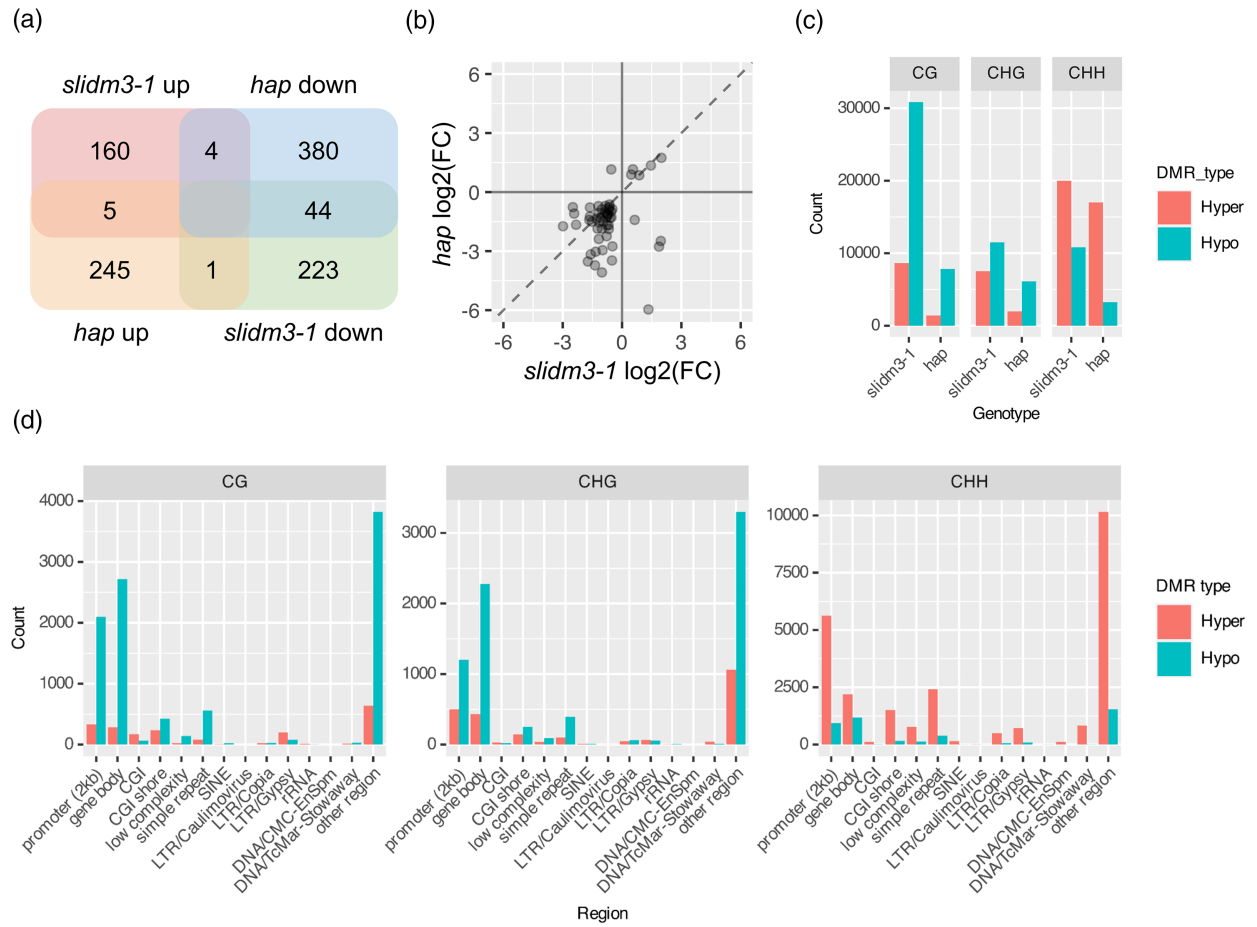

Figure 7. Comparison of the *slidm3-1* and *hap* transcriptome and DNA methylome.
(A) Overlap of the differentially expressed genes (DEGs) we identified in the *slidm3-1* and the *hap* mutant (B) Comparison of the log2-transformed fold-changes of the common DEGs (the genes in the intersections in panel A) in the *hap* and *slidm3-1* mutants. Every dot represents a gene. If a gene is changed to the same extent in both mutants, the dot should appear along the dashed line. Spearman's rank correlation test revealed a weak positive correlation ($\rho = 0.243$, $P = 0.077$).
(C) Summary statistics of the differentially methylated regions (DMRs) identified in the *slidm3-1* and the *hap* mutants by sequence context. Hyper and Hypo means hyper- and hypomethylated DMRs.
(D) Overlap of the *hap* DMRs with various genomic features by sequence context. See legend of Figure 5 for feature descriptions.

conducted hypergeometric tests. The overlaps containing the above-mentioned 44, 5, 4 and 1 genes were 13.3, 4.1, 1.9, and 0.5 times higher than expected by chance (*P*-values: 5.97e-36, 0.008, 0.157 and 0.858), respectively. These results indicate that the overlaps involving downregulated genes in both mutants, as well as upregulated genes in both mutants, were statistically significant ($P < 0.05$). In contrast, the overlaps involving genes with opposing expression patterns were likely due to random chance. This suggests that SIIDM3 and HAP likely target common downstream genes.

When we plotted the fold-changes of gene expressions in the two mutants against each other, we observed that only a few genes changed to a similar extent in the two mutants (dots along the dashed line in Figure 7b). A Spearman's rank correlation test indicated a weak positive correlation between *slidm3-1* and *hap* DEGs ($\rho = 0.243$), but this correlation was not statistically significant ($P = 0.077$). The Gene Ontology term enrichment analysis of the downregulated *hap* DEGs gave a very similar result to the *slidm3-1* analysis (Table S4k). We investigated if the common DEGs have some GO terms enriched compared with the union of the DEGs in the two mutants. One term 'oxidation–reduction process' (GO:0055114) was enriched with nine genes. These genes might be involved in the secondary metabolite production of the hairs, hormone metabolism, or ROS levels that could affect stress response.

Analysing the *hap* DNA methylome data, we identified 51 817 DMRs altogether (versus the 112 911 DMRs in *slidm3-1*) of which 2023 were CG-hyper-DMR, and 9991 CG-hypo-DMR, 2483 CHG-hyper-DMR and 7685

CHG-hypo-DMR, 25117 CHH-hyper-DMR and 4518 CHH-hypo-DMR (Figure 7c). This pattern was similar to the one identified in the *slidm3-1* mutant, namely, there were more hypo-DMRs in the CG and CHG context and more hyper-DMRs in the CHH context. The genomic location of the *hap* DMRs were also similar to the DMRs in the *slidm3-1* mutant (Figure 7d). Most of the DMRs were associated either with genes (promoter and gene body regions) or intergenic regions that were not associated with transposons or repeat elements ('other region' in the figure).

When we analysed the overlap between *hap* and *slidm3-1* DMRs associated with promoter regions and gene bodies, irrespective of sequence context, DMR type and DEG association, only a moderate overlap was observed between the two mutants. Specifically, 1307 and 1322 intersections were identified for promoter-associated and gene body-associated DMRs, respectively. The corresponding Jaccard indices (ratio of the intersection to the union of the DMR sets) were 0.037 and 0.034, indicating limited overlap. However, these overlaps were 35.586 and 28.381 times higher than expected by chance as measured by Fisher's exact tests ($P \approx 0$ in both cases).

To delve deeper into the functional implications of the limited but significant overlap in promoter and gene body-associated DMRs between the *slidm3-1* and *hap* mutants, we analysed the Gene Ontology (GO) terms associated with genes harbouring these DMRs. When focusing on genes with promoter DMRs, we identified a single shared GO category between the two mutants: 'ADP-binding' (GO:0043531) (Figure 8a). This category is exclusively composed of nucleotide-binding site and leucine-rich repeat domain-containing (NBS-LRR) proteins, which are key players in immune response (Marone et al., 2013). In contrast, genes with DMRs in their gene bodies shared 29 GO categories (Figure 8a,b), with half of them being associated with the higher-level 'catalytic activity' category (GO:0003824) (Figure 8b). Notably, the 'ADP-binding' category was also shared by genes with gene body DMRs. To explore potential regulatory mechanisms, we examined the 'cell communication' category (GO:0007154). This category encompasses genes with diverse functions, including transcription factors, small GTPase signalling components, various protein kinases (including NBS-LRR proteins), auxin signalling components, photoreceptors, and other proteins all of which can be related to trichome developmental regulation. A comparison of the gene content within this category revealed 73 overlapping genes between the two mutants (Figure 8c). To determine whether these overlapping genes differed from non-overlapping ones, we performed a GO term enrichment analysis using the union set of genes in this category as a reference. Two related GO categories were enriched: 'nucleic acid binding' (GO:0003676) and 'DNA binding' (GO:0003677), primarily comprising MADS-box transcription factors and two-component response regulators with DNA-binding domains (Figure 8d,e). MADS-box transcription factors are known to regulate developmental pattern formation and stress responses (Castelán-Muñoz et al., 2019; Gramzow & Theissen, 2010) while the two component system is involved in cytokinin hormone signalling (Mason et al., 2004) and also in stress responses (Grefen & Harter, 2004). The expression of these genes in our dataset remained unchanged in both *slidm3-1* and *hap* mutants. It is important to note that epigenetic regulation often establishes a permissive or restrictive chromatin environment, which may not always manifest in immediate gene expression changes. Additionally, DNA methylation can exhibit greater stability than gene expression alterations. A compelling example is a gene called *SlARR-B9* (Wang et al., 2020) encoding a B-type two-component response regulator with a Myb-SANT DNA-binding domain (gene ID in SL3.0 genome assembly is Solyc07g009575.1, while in SL4.0, it is called Solyc07g009580.2). This gene harbours a hypo-CHH DMR at its exon–intron junction site in both mutants (Figure 8f), suggesting potential DNA methylation-regulated alternative splicing. It should be noted that the methylation pattern in the two mutants were remarkably similar despite the fact that the samples derive from two different labs, tissues and growth conditions. While our dataset shows no expression of this gene, the concordant DNA methylation site and its methylation level in both mutants suggest active regulation and potential expression in specific, possibly underrepresented cell types like hair tips or initial cells. This notion is supported by the very low expression of *SlARR-B9* across various tissues, with the highest levels observed in young leaves (Wang et al., 2020). Intriguingly, a similar Type-B response regulator gene (RR22) has been implicated in rice trichome development (Worthen et al., 2019; Yamburenko et al., 2020). Further research is needed to explore the potential regulatory role of the *SlARR-B9* gene in tomato hair development.

Taken together, we have shown that the tomato IDM3 protein was associated with proteins that might form a chromatin remodelling complex at hypermethylated DNA regions, and that the lack of a functional *SlIDM3* gene altered the global DNA methylome and transcriptome that could potentially lead to altered trichome development.

DISCUSSION

Increased DNA Methylation 3 (IDM3) protein was originally identified in complex with MBD7, IDM1, IDM2 in *Arabidopsis* (Lang et al., 2015; Li et al., 2015). The *Arabidopsis* IDM complex inhibits DNA hypermethylation at some genomic regions and prevents transcriptional gene silencing. Promoter methylation is mainly, although not exclusively, associated with gene repression (Law & Jacobsen, 2010). Methylation at TEs may spread to and silence adjacent,

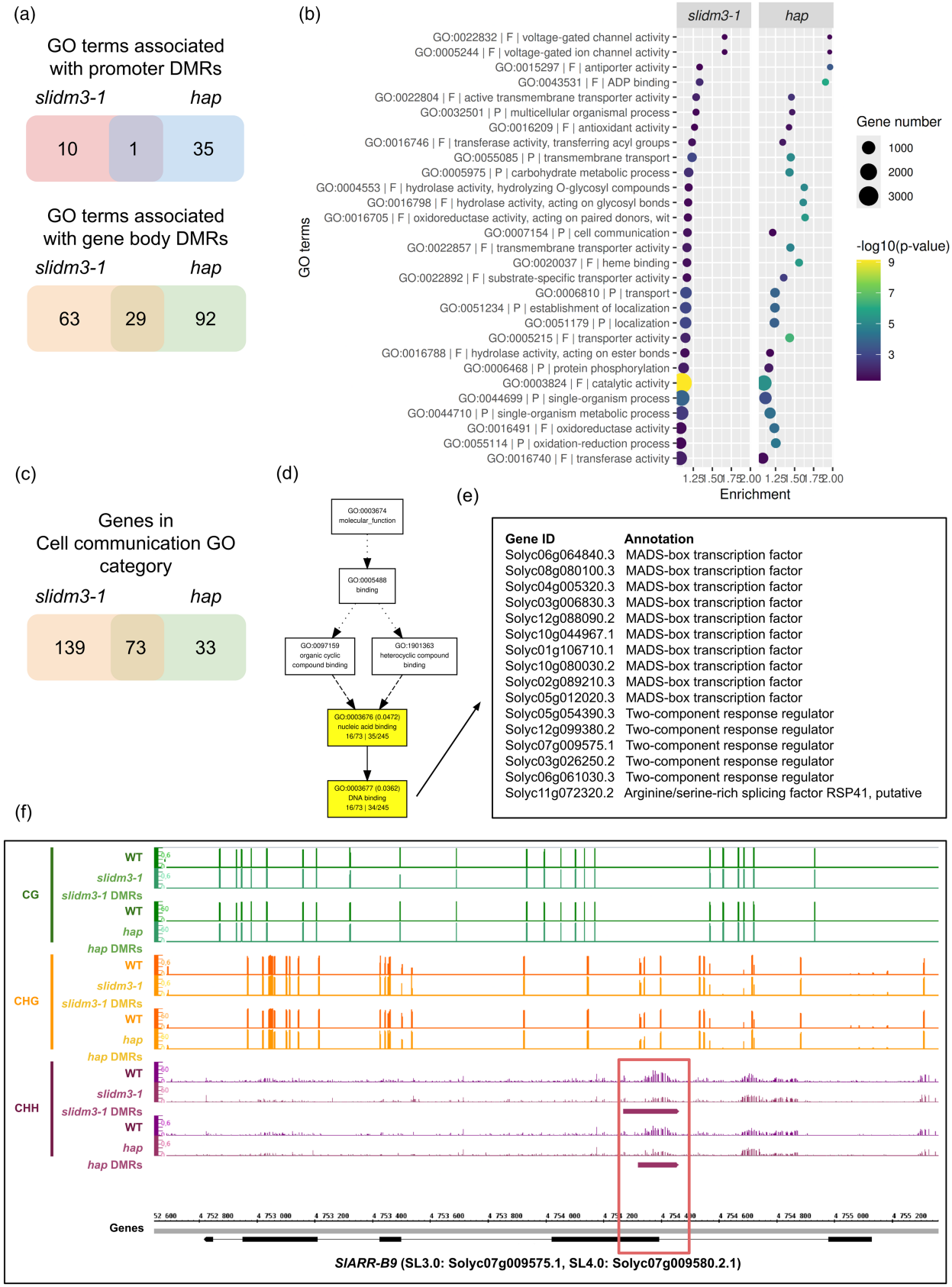

Figure 8. Functional analysis of the genes with differentially methylated regions in their promoters and gene bodies.
(A) Gene Ontology term enrichment analysis of the *slidm3-1* and *hap* DMRs located either in the promoter or gene body regions. The intersection of the GO terms were determined by Venn analysis.
(B) The 29 common GO categories in the gene body DMR containing genes. The letters P or F in the name of GO terms refer to Biological Process and Molecular Function GO terms, respectively. The Enrichment factor was calculated by dividing the ratio of the genes of the given category within the submitted genes by the ratio of the genes in that category in the reference gene set.
(C) Gene content of the GO category cell communication in the two mutants.
(D) GO term enrichment analysis of the 73 common genes in cell communication category compared with the union of the genes in the same category in the two mutants.
(E) List of the genes in the DNA-binding category.
(F) Genome browser snapshot of the cytosine methylation levels in the *slidm3-1* and the *hap* mutants across the genomic region containing the Myb-SANT domain containing two-component regulator gene called *SlARR-B9* (Wang et al., 2020) the gene ID of which in the SL3.0 genome assembly is Solyc07g009575.1, while in the 4.0 version, it is Solyc07g00580.2. Each track shows the mean of three biological replicates from both the *slidm3-1* and the *hap* data series. The red square shows the hypo-CHH DMRs in the two mutants at the exon–intron junction at exon 2 (black bars show exons, black lines between them show introns). Note the remarkably similar methylation pattern in the two mutants despite the fact that the samples derive from two different labs, tissues and growth conditions.

transcriptionally active genes (Tang et al., 2016; Yamamuro et al., 2014). It was shown that MBD7 associates with methylated DNA and recruits other anti-silencing factors to create a permissible chromatin environment for binding of DNA demethylases (Lang et al., 2015). These observations suggested that MBD7 and the IDM proteins limit the spread of DNA methylation by promoting active DNA demethylation (Lang et al., 2015; Li et al., 2015). Although the components and the function of the IDM complex was characterised in detail in the model plant *Arabidopsis*, the agriculturally important tomato IDM complex remained unidentified. Active demethylation was shown to play a role in tomato fruit ripening (Lang et al., 2017; Liu et al., 2015) suggesting that the tomato IDM complex was also involved in the regulation of this process. We found that the expression of the tomato homologue of the *Arabidopsis* IDM3 was induced during fruit ripening, similarly to the induction of *SlDML2*. We created homozygous *slidm3* mutants by CRISPR-Cas9-based genome editing hoping that we would observe a fruit ripening phenotype but we could not observe any. However, we noticed that the mutant plants had more Type I glandular trichomes than the wild-type plants along with some trichome developmental defects that were similar to the phenotype of the recently identified *hairplus* (*hap*) mutant.

To identify the components of the tomato IDM complex, we immuno-purified the SlIDM3-GFP interacting proteins from tomato vegetative stems and leaves and analysed them with mass spectrometry. We showed that SlIDM3 interacted with HAP (SlSUVH3), SlIDM2, SlMBD5 and SlDNAJ1 proteins (Table 1; Table S1). We confirmed these interactions in a heterologous *Agrobacterium*-mediated leaf infiltration system (Figure 3). These results suggest that SlIDM3, along with SlMBD5, HAP (SlSUVH3), SlDNAJ1 and SlIDM2 may form a putative IDM complex in tomato that could influence trichome development by regulating active DNA demethylation at certain genomic loci. SlIDM3 is localised in cell nuclei (Figure S4) and its mutation results in genome-wide alteration of DNA methylation pattern, consistent with its putative epigenetic regulatory role. Since no fruit ripening phenotype was observed in the *slidm3* mutants, it is possible that IDM complex(es) other than the one we identified may exist that could regulate fruit ripening. This possibility is also supported by the fact that all the components we identified in our complex are members of multigene families with possible divergent roles. Also, there are four DNA demethylases in tomato and only one of them (SlDML2) was described as a regulator of fruit ripening so far (Lang et al., 2017; Liu et al., 2015) while no information is available about the function of the other three SlDMLs. It is possible that one or more of them may regulate trichome development.

The IDM demethylase complex subunits perform well-defined roles. IDM3 and IDM2 are α-crystallin domain proteins that may act as scaffold or structural units within the IDM complex; besides, they may act as chaperones that help folding of the other subunit proteins (Lang et al., 2015). In tomato, there are 50 genes encoding α-crystallin domain proteins (Paul et al., 2016) and four of them belong to a clade containing *SlIDM3* and *SlIDM2*.

SlMBD5 is a methyl-CG binding domain protein (MBD) and previously it was shown to be targeted to the nucleus. Furthermore, electrophoresis mobility shift analysis showed that the MBD domain of SlMBD5 specifically binds to DNA that contains methylated cytosines in the CG context but not to cytosines in the CHG or CHH contexts. When expressed in protoplasts, SlMBD5 was capable of activating transcription of CG islands (Li et al., 2016). SlMBD5 is also a member of a gene family containing 18 MBD genes (Parida et al., 2018).

HAP/SlSUVH3 is homologous to a group of SET domain-containing SUVH proteins (Aiese Cigliano et al., 2013) linked to epigenetic control of the expression of genes including *ROS1* (Harris et al., 2018; Xiao et al., 2019). SUVH family proteins bind methylated DNA in a sequence context dependent manner (Li et al., 2018). It was shown that HAP/SlSUVH3 similarly to its *Arabidopsis* homologues (SUVH1 and SUVH3) does not have histone

methyltransferase activity (Fonseca et al., 2022). However, it has been demonstrated that in *Arabidopsis*, SUVH1 and SUVH3 interact with the DNAJ domain-containing proteins forming a protein complex that binds to methylated DNA sites near TEs, inducing the demethylation and transcriptional activation of adjacent genes (Harris et al., 2018; Xiao et al., 2019; Zhao et al., 2019). The function of *HAP*/*SlSUVH3* gene was identified in tomato. The tomato *HAP* gene controls Type I glandular trichome density and *hap* loss-of-function mutation induces a large number of epigenetic changes (DNA demethylation) in the tomato genome (Fonseca et al., 2022). We have shown here that HAP is part of a SlIDM3 containing protein complex and in agreement with this, both the *hap* and *slidm3* mutant tomato plants exhibit the same high Type I trichome density phenotype. Furthermore, *slidm3* mutant plants show genome scale epigenetic changes very similar to that of the *hap* mutant (Figure 7).

SlDNAJ1 is a putative transcriptional activator. It was shown previously that ectopic recruitment of *Arabidopsis* DNAJ1 enhanced gene transcription in plants, yeast, and mammals (Harris et al., 2018). In *Arabidopsis* SUVH1 and SUVH3 are required to recruit DNAJ1 and DNAJ2 to methylated DNA. It was also shown that SUVH1, SUVH3, DNAJ1 and DNAJ2 are localised at RdDM sites in *Arabidopsis*. Therefore, it was proposed that SUVH1 and SUVH3 in complex with DNAJ1 and DNAJ2 evolved to counteract the repressive effect of TE insertion near genes (Harris et al., 2018).

There are conflicting data regarding the role of the IDM3-containing chromatin remodelling complexes. IDM3 (together with SUVH and DNAJ proteins) functions as a DNA methylation reader complex component to trigger ROS1-mediated DNA demethylation in *Arabidopsis* (Duan et al., 2017; Lang et al., 2015). On the other hand, IDM3 was also shown to be needed for establishment or maintenance of DNA methylation; IDM3 loss-of-function allele led to genome-wide DNA methylation loss at specific genomic loci (Miao et al., 2021). The *Arabidopsis*, IDM3 interacts with RDM1 and DMS3, therefore, it was suggested that IDM3 may participate in DNA methylation through RdDM (Miao et al., 2021). The seemingly contradictory roles of IDM3 (DNA demethylation *versus* methylation activities), therefore, may depend on protein complex composition and could reflect the existence of a competition between DNA methylation and demethylation effectors. Components of the RdDM pathway (RDM1, DMS3 or others); however, were not enriched in our IP-MS dataset. The reason for this could be that RdDM-related alternate IDM3-containing protein complexes may present in tissues or developmental stages other than our samples derived from.

Alternatively, the DNA methylation and demethylation may be indirectly connected, for example, DNA demethylation of certain sites that normally should be in a hypermethylated state would trigger *de novo* methylation genome-wide. This is how the 'methylstat' works in *Arabidopsis* (Lei et al., 2015; Xiao et al., 2019): the promoter of ROS1 DNA demethylase contains a transposon that should be hypermethylated to allow *ROS1* expression. This region is a ROS1 target, therefore, when ROS1 level is high, the hypermethylated region is demethylated, which in turn causes the *ROS1* expression to drop. The hypomethylated state of this region triggers *de novo* methylation by RdDM which restores the hypermethylated state and *ROS1* expression. This region is not the only target of ROS1, the demethylation affects thousands of other sites in the genome which triggers *de novo* methylation by RdDM at these sites. We speculate that the same methylstat should work in tomato as well, although not necessarily in the same way, that is, the methylation sensor region may reside in the promoter of other DNA demethylation or RdDM-related genes. Such a methylstat mechanism has not been described in tomato yet, although a recent study suggested that one of the four tomato DNA demethylases, SlDML1, might be a part of it (Bianchetti et al., 2020). Although we could not identify the methylstat using the *slidm3-1* and *hap* datasets, we think that the observed bias of methylation status by sequence context could be a sign of a methylstat mechanism.

Gene body methylation cannot be directly linked to transcriptional changes; however, it was shown that it can affect the inducibility or the transcriptional plasticity of genes. Gene bodies of constitutively expressing genes ('housekeeping genes') are fully methylated in the CG context while they are void of CHG or CHH methylation. Inducible genes, however, are hypomethylated in all sequence contexts (Coleman-Derr & Zilberman, 2012; Zilberman et al., 2008). A recent study revealed a third group of genes that contain heterogeneously methylated cytosines in CG context (Williams et al., 2023). These genes were found to display a higher level of gene expression plasticity than other genes either with fully methylated or not methylated gene bodies. The mentioned genes are dynamically targeted by active DNA demethylation and *de novo* methylation (in the CG context) and when DNA demethylases are missing (in the *ddrd* mutant) they display a gene body methylation pattern similar to the constitutively expressing ('housekeeping') genes, namely, they are fully methylated. We observed mainly gene body hypomethylation in the CG context (especially in the *hap* mutant) and hypermethylation in the CHH context which suggests that the situation is the opposite in our mutants than in the DNA demethylase mutants in *Arabidopsis*, namely, DNA demethylation is not missing but hyperactive, which results in a hypomethylation in all contexts, that triggers *de novo* DNA methylation only in the CHH context by RdDM.

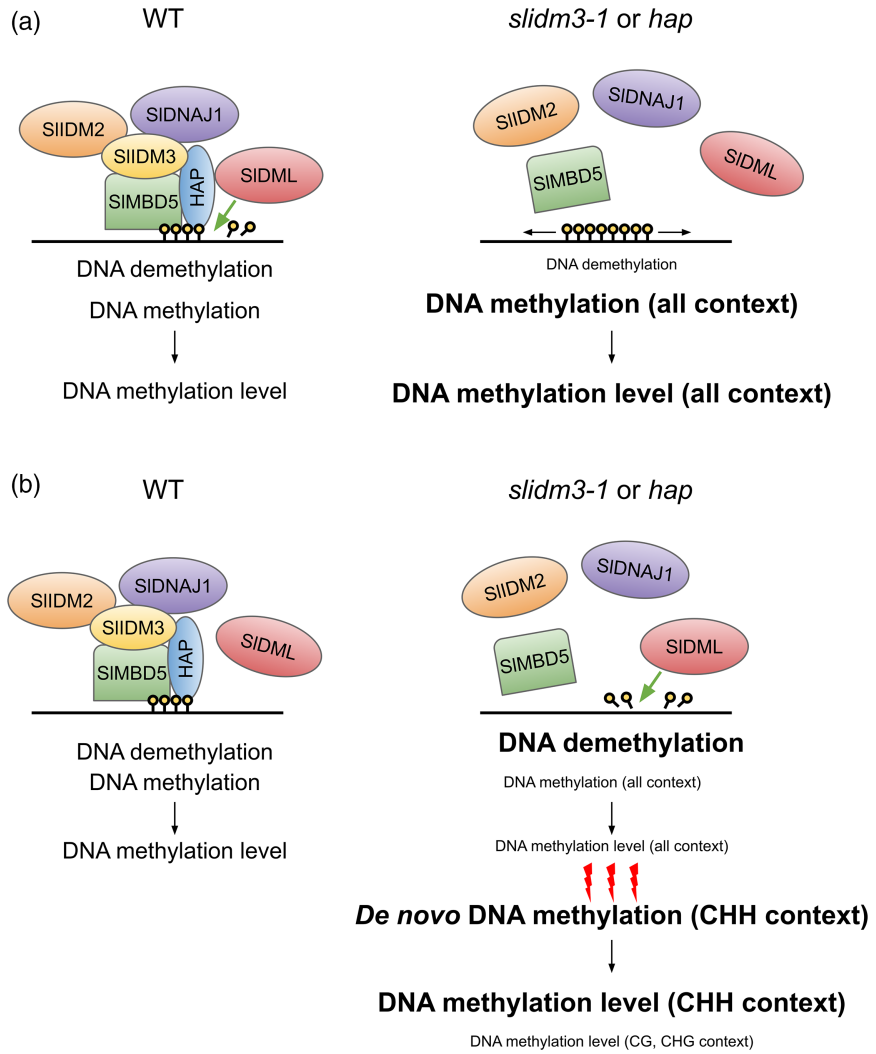

Figure 9. Schematic models of the tomato IDM complex.
(A) In the first scenario, similarly to the *Arabidopsis* IDM complex, the hypothetical tomato IDM complex binds hypermethylated DNA at certain regions promoting their demethylation. SIMBD5 and possibly HAP (SISUVH3) bind methylated DNA directly while SlIDM3 serves as a bridge between the methyl DNA-binding components and the rest of the complex. The lack of functional SlIDM3 or HAP could lead to the hypermethylation of the regions in all sequence contexts (CG, CHG, CHH).
(B) To explain the observed bias in methylation in the CHH context (mostly hypermethylation) versus the CG and CHG contexts (mostly hypomethylation) in both the *slidm3-1* and the *hap* mutant, we formulated an alternative hypothesis. According to this, the complex we identified works differently to the *Arabidopsis* IDM complex, it prevents the hypermethylated regions from demethylation. The lack of functional IDM3 or HAP could lead to the demethylation of the regions that are hypermethylated in the wild-type plants in all the three possible sequence contexts (CG, CHG, CHH). This could trigger a countereffect, a genome-wide *de novo* DNA methylation in the CHH sequence context at sites that should be normally hypermethylated. As a result, we can observe residual hypomethylation in the CG and CHG context, and mostly hypermethylation in the CHH context.

Based on our results and the literature, we can form hypothetical models of the tomato IDM complex actions (Figure 9). According to one model, similarly to the current model of the *Arabidopsis* IDM complex, the tomato IDM complex positively regulates DNA demethylation at certain hypermethylated sites (Figure 9a). In this model, SlIDM3 forms a protein complex with HAP, SlIDM2, SlMBD5 and SlDNAJ1 at certain hypermethylated sites leading to their targeted demethylation by DNA demethylases. The lack of *SlIDM3* or *HAP* in the *slidm3-1* mutant causes cytosine hypermethylation in all sequence contexts at hundreds of loci in the euchromatic regions. Alternatively, the protein complex we identified may be different to its *Arabidopsis* counterpart and may have a negative regulatory role in the DNA demethylation process (Figure 9b). According to this alternative hypothesis, this complex blocks the demethylation of the hypermethylated sites in the WT plants. The lack of functional *SlIDM3* or *HAP* could prevent the assembly of this IDM complex allowing DNA cytosine demethylation in all the three sequence contexts which could

eventually trigger *de novo* DNA methylation in the CHH context to ensure the hypermethylation of the marked sites. In our hypothetical model, similarly to the *Arabidopsis* IDM complex, we assume that the identified interacting proteins form a single large protein complex, however, we cannot rule out the possibility of the existence of more than one IDM3-containing complexes.

The disturbed balance between DNA methylation and demethylation could alter the expression of some genes that regulate trichome development which would subsequently result in a hairy phenotype. Such candidate is the Myb-SANT domain-containing two-component response regulator *SlARR-B9*, the alternative splicing of which might be regulated by DNA methylation. To reveal the exact epigenetic regulation of trichome development in the *slidm3-1* mutant, further work is required.

EXPERIMENTAL PROCEDURES

Plant material and growth conditions

Solanum lycopersicum cultivar Moneymaker was used as wild-type (WT). Tomato plants were grown in a greenhouse under long day conditions (16 h light, 8 h dark). Tobacco (*Nicotiana benthamiana*) plants used for transient co-immunoprecipitation (co-IP) were grown in a growth chamber with controlled light and temperature (16 h day, 8 h night, 24°C). For tomato transformation, Moneymaker seedlings were germinated on sterile MS medium, in a growth chamber (16 h day, 8 h night; 25°C and 18°C, respectively) for 10 days.

Sample preparation for the WGBS and RNAseq experiments

For the WGBS and RNAseq experiments, vegetative stem samples (third internode counted from the top) were collected from 6-week-old WT and *slidm3-1* plants grown in the greenhouse in three biological replicates. Every replicate consisted of three pieces of stems from different individuals. Each stem was split into half, one half was used for DNA and one for RNA isolation.

Molecular cloning

To design CRISPR/Cas9 guide sequences targeting *SlIDM3* (Solyc04g082720), we used the CRISPOR server (http://crispor.tefor.net; Haeussler et al., 2016). To create a CRISPR/Cas9-based knock-out gene construct, we followed the protocol described by Rodríguez-Leal et al. (2017) utilising modular cloning and the principle of GoldenGate assembly (Engler et al., 2014). For this, we used the MoClo Toolkit (Werner et al., 2012). The individual guide RNAs were PCR amplified with Phusion™ Hot Start II DNA Polymerase (Thermo Scientific, Waltham, MA, USA) using the template pICH86966_AtU6-sgRNA-PDS (Addgene) in an overlap extension PCR in which the overlapping part was the 20 bp guide sequence and the two halves were the U6 promoter and the scaffold RNA with the U6 terminator. The PCR primers contained *Bsa*I recognition sites to be able to clone the product into the pICH47751 vector with the Golden Gate assembly method. Next, the kanamycin resistance module in pICH47732 (Addgene), the Cas9 module in pICH47742 (Addgene), and the gRNA module in pICH47751 were cloned into pAGM4723 along with the end-linker pICH79277 in a Golden Gate reaction. Primers are listed in Table S1.

For the *35S:GFP* and *35S:SlIDM3-GFP* and for the constructs used in the co-IPs, derivatives of the Bin61S binary vector (Bin-HA, Bin-MYC and Bin-mGFP4) were used (Kertész et al., 2006). The appropriate intronless coding sequences were amplified with Phusion™ Hot Start II DNA Polymerase (Thermo Scientific, Waltham, MA, USA) from a cDNA library prepared from wild-type Moneymaker tomato stems using the primers described in Table S1. The PCR products and vectors were digested with the appropriate restriction enzyme as noted in Table S1 and after ligation, transformed into *E. coli*. The sequences of the gene constructs were validated by Sanger sequencing. The eRF3-MYC construct was previously described (Auber et al., 2018; Nyikó et al., 2017).

Plant transformation

The genome editing constructs, the *35S:GFP*, and the *35S:SlIDM3-GFP* constructs were transformed into *Agrobacterium tumefaciens* strain LB4404 competent cells with the freeze–thaw method (Chen et al., 1994). Moneymaker tomato plants were transformed using an *Agrobacterium tumefaciens*-mediated transformation method described earlier (Fernandez et al., 2009). We selected homozygous plants by sampling different parts of the plants, and then mixing them for PCR and sequencing. Genomic DNA for genotyping was purified as described in the DNA and RNA extraction part of the Materials and Methods. Primers used for genotyping were listed in Table S4. Homozygous lines were used for phenotypic and molecular characterisation.

Optical microscopy

For trichome observation, we selected 6-week-old tomato plants for study. We compared the trichome density of WT and *slidm3-1* mutant stems using the third internodes (the internode next to the meristem was counted as the first one and the internode close to hypocotyls as the last one). The stem samples from 6-week-old plants were observed under the confocal microscope Leica SP8 LIGHTNING and digital microscope Keyence VHX-5000.

Scanning electron microscopy

Trichome number and morphology were analysed in vegetative stems, using the third internodes of 6 weeks old mutant and wild-type plants. Five mutant and five control plants were analysed by scanning electron microscopy. Briefly, samples were fixed in 2% glutaraldehyde (100 mM phosphate buffer, pH 7.2) and after washing them in the same buffer, samples were dehydrated in increasing ethanol gradient, transferred to amyl acetate, and completely dried by CO_2 critical point dryer equipment (Polaron CPD 7501). Finally, samples were gold-coated in a Zeiss HBA 1 vacuum evaporator and visualised in a Hitachi S-2360 N scanning electron microscope. Trichome counts were performed on at least 20 images obtained from 10 randomly chosen samples per genotypes. Type I–VII trichomes were counted.

Fluorescent protein immunoprecipitation (FP-IP) and mass spectrometry analysis

Total proteins from the third internodes of frozen 6 weeks old tomato stems expressing *35S:GFP* control or *35S:SlIDM3-GFP* fusion constructs were extracted as described (Kobayashi et al., 2015). Total protein extracts (4 mg/IP) were immuno-purified using anti-GFP antibody coupled magnetic beads (μMACS™ GFP

Isolation Kit, Miltenyi Biotec Inc, Auburn, USA, #130-091-125) digested in column with trypsin, and analysed in a single run on the mass spectrometer (Hubner et al., 2010). The resulting tryptic peptide mixture was desalted prior to LC–MS/MS analysis on a C18 ZipTip (Omix C18 100 μL tips, Varian), and the purified peptide mixture was analysed by LC–MS/MS using a nanoflow RP-HPLC (LC program: linear gradient of 3%–40% B in 100 min, solvent A: 0.1% formic acid in water, solvent B: 0.1% formic acid in acetonitrile) on-line coupled to a linear ion trap-Orbitrap (Orbitrap-Fusion Lumos, Thermo Fisher Scientific, Waltham, MA, USA) mass spectrometer operating in positive ion mode. Data acquisition was carried out in data-dependent fashion, the 20 most abundant, multiply charged ions were selected from each MS survey for MS/MS analysis (MS spectra were acquired in the Orbitrap, and CID spectra in the linear ion trap). Data interpretation: Raw data were converted into peak lists using the in-house Proteome Discoverer (v 1.4) and searched against the Uniprot *Solanum lycopersicum* (SOLLC) database (downloaded 2019.6.12, 37 006 proteins) using our in-cloud Protein Prospector search engine (v5.15.1) with the following parameters: enzyme: trypsin with maximum two missed cleavage; mass accuracies: 5 ppm for precursor ions and 0.6 Da for fragment ions (both monoisotopic); fixed modification: carbamidomethylation of Cys residues; variable modifications: acetylation of protein N-termini; Met oxidation; cyclisation of N-terminal Gln residues, allowing maximum two variable modifications per peptide. Acceptance criteria: minimum scores: 22 and 15; maximum *E* values: 0.01 and 0.05 for protein and peptide identifications, respectively. Spectral counting was used to estimate relative abundance of individual proteins in the GFP overexpressing negative controls (Jankovics et al., 2018).

Protein immunoprecipitation (IP) and western blot

For the Agroinfiltration assay, the Bin-HA, Bin-MYC and Bin-mGFP4 vectors carrying the tagged versions of genes of interest were directly transformed into the competent cells of *Agrobacterium tumefaciens* strain C58C1 by the freeze–thaw method (Chen et al., 1994). Wild-type, 3-week-old *N. benthamiana* leaves were infiltrated with a mixture of different Agro Bacterial cultures (OD_{600} of each culture was 0.4). The Agroinfiltration assays were performed as described earlier (Kertész et al., 2006). Briefly, 3 days post-infiltration (3 dpi), 1 g agroinfiltrated leaf patches were frozen in liquid N_2 and protein extraction was carried out using a lysis buffer (4 mL buffer/1 g plant material) containing: 100 mM Tris–HCl pH 7.6, 10 mM EDTA, 10 mM $MgCl_2$, 1% 2-mercaptoethanol, 0.05% sodium lauryl sarcosine. The lysis buffer was supplemented with one oComplete protease inhibitor tablet (Merck Millipore, Burlington, USA, #11697498001) before use. IP was carried out as described earlier (Baumberger & Baulcombe, 2005), except that G-25 separation was omitted and we used another IP buffer optimised for nuclear protein extraction: 100 mM Tris–HCl pH 7.6, 10 mM EDTA, 10 mM $MgCl_2$, 1% 2-mercaptoethanol, 1 piece of protease inhibitor tablet (Roche, Basel, Switzerland). Briefly the homogenised lysate was centrifuged 3 × 10 min at maximum 14 000 rpm until we get clear plant lysate. 1 mL from this clear plant lysate was added to 50 μL of Anti-c-MYC Agarose Affinity Gel antibody produced in rabbit (Merck Millipore, Burlington, USA, #A7470) or GFP Magnetic beads (μMACS™ GFP Isolation Kit, Miltenyi Biotec Inc, Auburn, USA, #130–091-125) and incubated for 1 h at 4 °C with continuous shaking (1400 rpm). Protein samples were resolved on 12% TGX Stain-Free™ FastCast™ Acrylamide Kit (Bio-Rad Laboratories, Hercules, CA, USA, #1610185) and transferred to PVDF membrane (Bio-Rad Laboratories, Hercules, CA, USA, #1620177). Transfer and subsequent processing of the membranes were performed according to the manufacturer's instructions. The following antibodies were used: HRP conjugated anti-GFP antibody (Miltenyi Biotec Inc, Auburn, USA, #130–091-833), HRP conjugated anti-HA and anti-c-myc antibodies (Merck Millipore, Burlington, USA, #12013819001 and #11814150001, respectively). For detection, the Clarity Western ECL substrate (Bio-Rad Laboratories, Hercules, CA, USA, #1705061) was used. Western blots were imaged on a ChemiDoc™ MP Imaging System and its own ImageLab™ v5.1 software (Bio-Rad Laboratories, Hercules, CA, USA).

Genomic DNA and total RNA purification

For both the DNA and RNA purification, 100 mg stem sample frozen in liquid nitrogen was homogenised in a pre-chilled mortar with a pestle. Either a mixture of 750 μL DNA extraction buffer (5 M urea, 50 mM Tris–HCl pH 7.6, 300 mM NaCl, 20 mM EDTA, 0.5% SDS, 2% sarkosyl, 0.1% sodium metabisulphite) and 600 μL phenol (pH 8.0) or 750 μL RNA extraction buffer (100 mM glycine-NaOH pH 9.0, 100 mM NaCl, 10 mM EDTA, 2% SDS) and 600 μL of phenol (pH 4.3) pre-warmed at 65 °C in a 1.5 mL tube was poured onto the sample, mixed thoroughly with the pestle and the liquid was transferred back to the tube, shaken vigorously, and centrifuged at maximum speed for 5 min. About 500 μL of the upper phase was transferred into a new tube and 500 μL phenol:chloroform:isoamyl alcohol (25:24:1, pH 8.0 or pH 4.3) was added, shaken vigorously, and centrifuged at maximum speed for 5 min. About 400 μL of the upper phase was transferred into a new tube, then 40 μL 3 M sodium-acetate (pH 5.2) and 800 μL (for DNA samples) or 1 mL (for RNA samples) ethanol was added. The samples were mixed thoroughly and incubated at −20°C for 1 h to precipitate nucleic acid. The precipitated nucleic acid was collected by centrifuging the tube at maximum speed at 4°C for 10 min, then the pellet was washed with 1 mL pre-chilled 70% ethanol two times. The pellet was dried in a SpeedVac, and resuspended in nuclease-free water. The DNA samples were treated with DNase-free RNase A (Thermo Fisher Scientific, Waltham, MA, USA, #EN0531) for 1 h at 37°C. After phenol/chloroform extraction and ethanol precipitation, the pellet was resuspended in nuclease-free water. The RNA samples was DNase I treated (Thermo Fisher Scientific, Waltham, MA, USA, #EN0521), phenol:chloroform extracted, precipitated in ethanol and resuspended in nuclease-free water. DNA and RNA integrity was determined by agarose gel electrophoresis and quantity was determined using a Nanodrop 2000 spectrophotometer (Thermo Fisher Scientific, Waltham, MA, USA).

DNA methylome and transcriptome sequencing

The library preparations and sequencing reactions were performed by Novogene (Cambridge, UK). For the DNA methylome (whole-genome bisulphite conversion, WGBS) libraries, the genomic DNA spiked with lambda DNA was fragmented to 200–400 bp. Half of the DNA samples were bisulphite treated to convert unmethylated cytosine into uracil while methylated cytosine stayed unchanged. Sequencing adapters were ligated, followed by second-strand DNA synthesis. The libraries were size selected and PCR amplified.

For the transcriptome libraries, the total RNA was first polyA selected and then sequencing libraries were prepared following the TruSeq® Stranded mRNA Library Prep protocol. For both types of sequencing, 150 bp paired-end sequencing reactions were performed by Novogene on a NovaSeq 6000 platform (Illumina, San Diego, USA).

Bioinformatic analysis of the WGBS data

First, FastQC v0.11.5 (Andrews, 2010) was used to perform basic statistics relevant to the quality of the raw reads. Thereafter, reads produced by the Illumina pipeline in FASTQ format were preprocessed through Trimmomatic v0.36 software (Bolger et al., 2014) using the following parameters: SLIDINGWINDOW:4:15 LEADING:3 TRAILING:3 ILLUMINACLIP:adapter.fa:2:30:10 MINLEN:36. After discarding unpaired reads, the remaining reads that passed all filtering steps were counted as clean reads and used in all subsequent analyses. Finally, FastQC was used to perform basic statistics on the quality of clean data reads.

Bismark software v0.16.3 (Krueger & Andrews, 2011) was used to perform alignments of bisulphite-treated reads to the tomato reference genome (version SL3.0 downloaded from the Ensembl database, not repeat masked version) with the following parameters: --score_min L,0,-0.2 -X 700 --dovetail. For this, the reference genome was first transformed into a bisulphite-converted version (C-to-T and G-to-A converted) and then indexed using bowtie2 (Langmead & Salzberg, 2012). Sequence reads were also transformed into fully bisulphite-converted versions (C-to-T and G-to-A converted) before they were aligned to similarly converted versions of the genome in a directional manner. Sequence reads that produced a unique alignment from the two alignment processes (original top and bottom strand) were then compared with the normal genomic sequence, and the methylation state of all cytosine positions in the read was inferred. The same reads that aligned to the same regions of the genome were regarded as duplicates. The sequencing depth and coverage were summarised using deduplicated reads (deduplicate_bismark --paired). The bisulphite nonconversion rate was calculated as the percentage of cytosine sequenced at cytosine reference positions in the lambda genome.

To calculate the methylation level (ML) of the sequence, sequences were divided into multiple bins, with a bin size of 10 kbp (Figure 4a) or 50 bp (Figure 4b). The sum of methylated and unmethylated read counts in each window was calculated. Methylation level (ML) for each C site shows the fraction of methylated Cs. It is defined as: ML (C) = reads (mC)/reads (mC) + reads (C). Calculated ML was further corrected with the bisulphite nonconversion rate according to previous studies (Lister et al., 2013). Given the bisulphite nonconversion rate r, the corrected ML was estimated as: ML (corrected) = ML $- r/1 - r$. The percentage of methylation levels was calculated as the proportion of mCs on the total C sites. The relative proportion of mCs in three contexts was calculated as the proportion of mCG, mCHG and mCHH on the total mC sites, respectively.

DMRs were identified using DSS software v2.12.0 (Feng et al., 2014; Park & Wu, 2016; Wu et al., 2015) with the following parameters: smoothing = TRUE, sequencing depth >1, smoothing.span = 200, delta = 0, p.threshold = 1e−05, minlen = 50, minCG = 3, dis.merge = 100, pct.sig = 0.5.

The overlaps of the DMRs with known genomic features were determined with bedtools v2.30.0 (Quinlan & Hall, 2010). Gene bodies were defined as the gene feature in the annotation file downloaded from https://ftp.ensemblgenomes.ebi.ac.uk/pub/plants/release-53/gff3/solanum_lycopersicum/Solanum_lycopersicum.SL3.0.53.gff3.gz, while promoters were the 2 kb regions upstream of the gene bodies and were extracted from the annotation file using the bedtools flank command. The annotation file containing the repeats and transposons was downloaded from the UCSC Genome Browser Gateway (https://hgdownload.soe.ucsc.edu/hubs/GCF/000/188/115/GCF_000188115.4/GCF_000188115.4.repeatMasker.out.gz) and reformatted to bed format. The extent of DMR overlaps was calculated using the Jaccard index as implemented in bedtools v2.31.1 (Quinlan & Hall, 2010). Hypergeometric tests (bedtools fisher) were used to determine the statistical significance of observed overlaps. Prior to analysis, DMRs within each sample were merged using bedtools merge.

Bioinformatic analysis of the RNA-seq data

As a first step of the transcriptome analysis, the reads were pseudoaligned to the tomato reference transcriptome v3.0.56 (downloaded from EnsemblPlants database, https://ftp.ensemblgenomes.ebi.ac.uk/pub/plants/release-56/fasta/solanum_lycopersicum/cdna/Solanum_lycopersicum.SL3.0.cdna.all.fa.gz) with kallisto v0.48.0 with the following parameters: -b 10 --bias. The differential expression analysis was performed with sleuth v0.30.0 using the default settings (Pimentel et al., 2017). Genes were considered differentially expressed if the Q-value was lower than 0.05. Transcription factors were identified using the list of tomato transcription factors downloaded from the PlantTFDB (http://planttfdb.gao-lab.org/download/TF_list/Sly_TF_list.txt.gz). The GO term enrichment analysis of the differentially expressed gene lists was performed with the AgriGO server v2 (http://systemsbiology.cau.edu.cn/agriGOv2; Du et al., 2010) using the default settings. Overlaps between the DEGs and DMRs were analysed with bedtools v2.31.1 (Quinlan & Hall, 2010) and the UpSetR R package v1.4.0 (Conway et al., 2017). The statistical analysis of the overlaps and the correlation of the DEG fold-changes were performed using the phyper and cor.test functions of the stats R package, respectively.

ACCESSION NUMBERS

Sequence data from this article can be found in the EnsemblPlants database (https://plants.ensembl.org/index.html) under the following accession numbers: SlIDM3, Solyc04g082720; SlIDM2, Solyc01g098810; SlDNAJ1, Solyc01g105780; HAP, Solyc10g077070; SlMBD5, Solyc11g068740.

ACKNOWLEDGEMENTS

This work was funded by the Hungarian Government Organisation NRDI (National Research, Development, and Innovation Office: https://nkfih.gov.hu/about-the-office) through the grants K-134974, K-143409 (to GySz), K-137722 (to TCs), FK-137811 (to PG), and PD-129119 (to TNy). T. Nyikó was supported by the Bolyai Scholarship (BO/00031/20/4).

CONFLICT OF INTEREST

The authors declare no conflict of interest.

DATA AVAILABILITY STATEMENT

Raw sequences from the WGBS and RNAseq experiments were deposited in the SRA database under the project number PRJNA974982.

SUPPORTING INFORMATION

Additional Supporting Information may be found in the online version of this article.

Figure S1. Tissue specific expression of *SlIDM3* and growth characteristic of the *slidm3-1* plant. RT-qPCR measurement of *SlIDM3*

expression in several tissues in WT tomato plants and pictures of the WT and *slidm3-1* plant grown in the greenhouse.

Figure S2. Morphological differences of trichomes between the WT and *slidm3-1* plants. Optical and electron microscopic pictures of the aberrant trichomes observed on *slidm3-1* plants.

Figure S3. HPLC measurement of acyl sugars from six-week-old WT and *slidm3-1* plants.

Figure S4. Intracellular localisation of the SlIDM3-GFP protein. Confocal fluorescent microscopic images of the SlIDM3-GFP signal in epidermal cells, trichomes, and guard cells.

Figure S5. Examples of spreading of methylation from TEs to the neighbouring regions in *slidm3-1*. Genome browser snapshots of two examples where the DNA methylation expands into the neighbouring regions in the promoter of genes in the *slidm3-1* mutant.

Figure S6. GO term enrichment analysis of the genes that were downregulated in the *slidm3-1* mutant. Significantly enriched GO term categories related to the Molecular Function category.

Figure S7. Intersections between the DEGs and promoter or gene body-associated DMRs. Showing all intersections between promoter and gene body associated differentially methylated regions (DMRs) with differentially expressed genes (DEGs) in the *slidm3-1* mutant compared to wild-type, non-intersecting included.

Data S1. Supporting Information.

Table S1. Primers. List of primers used for the cloning of the CRISPR guide RNAs, gene constructs, genotyping, and the RT-qPCRs.

Table S2. Mass spectrometry analysis of IDM3-GFP interacting proteins. List of identified SlIDM3-GFP interacting proteins with peptide coverages.

Table S3. WGBS analysis. Sequence statistics, list of identified differentially methylated regions with coordinates, length, number of cytosines, methylation levels, test statistics, sequence context, and annotation.

Table S4. Transcriptome analysis. Sequence statistics, list of differentially expressed genes with annotations, list of all genes with expressions, differentially expressed transcription factor genes, and the result of the GO term enrichment analysis.

REFERENCES

Aiese Cigliano, R., Sanseverino, W., Cremona, G., Ercolano, M.R., Conicella, C. & Consiglio, F.M. (2013) Genome-wide analysis of histone modifiers in tomato: gaining an insight into their developmental roles. *BMC Genomics*, **14**, 57. Available from: https://doi.org/10.1186/1471-2164-14-57

Andrews, S. (2010) FastQC: a quality control tool for high throughput sequence data [WWW Document]. Babraham Bioinforma. - FastQC Qual. Control Tool High Throughput Seq. Data. http://www.bioinformatics.babraham.ac.uk/projects/fastqc/

Auber, A., Nyikó, T., Mérai, Z. & Silhavy, D. (2018) Characterization of eukaryotic release factor 3 (eRF3) translation termination factor in plants. *Plant Molecular Biology Reporter*, **36**, 858–869. Available from: https://doi.org/10.1007/s11105-018-1128-5

Baumberger, N. & Baulcombe, D.C. (2005) Arabidopsis ARGONAUTE1 is an RNA slicer that selectively recruits microRNAs and short interfering RNAs. *Proceedings of the National Academy of Sciences of the United States of America*, **102**, 11928–11933. Available from: https://doi.org/10.1073/pnas.0505461102

Bianchetti, R., Luca, B.D., de Haro, L.A., Rosado, D., Demarco, D., Conte, M. *et al.* (2020) Phytochrome-dependent temperature perception modulates isoprenoid metabolism. *Plant Physiology*, **183**, 869–882. Available from: https://doi.org/10.1104/pp.20.00019

Bolger, A.M., Lohse, M. & Usadel, B. (2014) Trimmomatic: a flexible trimmer for Illumina sequence data. *Bioinformatics*, **30**, 2114–2120. Available from: https://doi.org/10.1093/bioinformatics/btu170

Castelán-Muñoz, N., Herrera, J., Cajero-Sánchez, W., Arrizubieta, M., Trejo, C., García-Ponce, B. *et al.* (2019) MADS-box genes are key components of genetic regulatory networks involved in abiotic stress and plastic developmental responses in plants. *Frontiers in Plant Science*, **10**, 853. Available from: https://doi.org/10.3389/fpls.2019.00853

Chalvin, C., Drevensek, S., Dron, M., Bendahmane, A. & Boualem, A. (2020) Genetic control of glandular trichome development. *Trends in Plant Science*, **25**, 477–487. Available from: https://doi.org/10.1016/j.tplants.2019.12.025

Chang, J., Yu, T., Yang, Q., Li, C., Xiong, C., Gao, S. *et al.* (2018) Hair, encoding a single C2H2 zinc-finger protein, regulates multicellular trichome formation in tomato. *The Plant Journal*, **96**, 90–102. Available from: https://doi.org/10.1111/tpj.14018

Chen, H., Nelson, R.S. & Sherwood, J.L. (1994) Enhanced recovery of transformants of agrobacterium tumefaciens after freeze-thaw transformation and drug selection. *BioTechniques*, **16**, 664–670.

Coleman-Derr, D. & Zilberman, D. (2012) Deposition of histone variant H2A.Z within gene bodies regulates responsive genes. *PLoS Genetics*, **8**, e1002988. Available from: https://doi.org/10.1371/journal.pgen.1002988

Conway, J.R., Lex, A. & Gehlenborg, N. (2017) UpSetR: an R package for the visualization of intersecting sets and their properties. *Bioinformatics*, **33**, 2938–2940. Available from: https://doi.org/10.1093/bioinformatics/btx364

Du, Z., Zhou, X., Ling, Y., Zhang, Z. & Su, Z. (2010) agriGO: a GO analysis toolkit for the agricultural community. *Nucleic Acids Research*, **38**, W64–W70. Available from: https://doi.org/10.1093/nar/gkq310

Duan, C.-G., Wang, X., Xie, S., Pan, L., Miki, D., Tang, K. *et al.* (2017) A pair of transposon-derived proteins function in a histone acetyltransferase complex for active DNA demethylation. *Cell Research*, **27**, 226–240. Available from: https://doi.org/10.1038/cr.2016.147

Engler, C., Youles, M., Gruetzner, R., Ehnert, T.-M., Werner, S., Jones, J.D.G. *et al.* (2014) A Golden Gate modular cloning toolbox for plants. *ACS Synthetic Biology*, **3**, 839–843. Available from: https://doi.org/10.1021/sb4001504

Ewas, M., Gao, Y., Ali, F., Nishawy, E.M., Shahzad, R., Subthain, H. *et al.* (2017) RNA-seq reveals mechanisms of SlMX1 for enhanced carotenoids and terpenoids accumulation along with stress resistance in tomato. *Scientific Bulletin*, **62**, 476–485. Available from: https://doi.org/10.1016/j.scib.2017.03.018

Ewas, M., Gao, Y., Wang, S., Liu, X., Zhang, H., Nishawy, E.M.E. *et al.* (2016) Manipulation of SlMXI for enhanced carotenoids accumulation and drought resistance in tomato. *Scientific Bulletin*, **61**, 1413–1418. Available from: https://doi.org/10.1007/s11434-016-1108-9

Feng, H., Conneely, K.N. & Wu, H. (2014) A Bayesian hierarchical model to detect differentially methylated loci from single nucleotide resolution sequencing data. *Nucleic Acids Research*, **42**, e69. Available from: https://doi.org/10.1093/nar/gku154

Fernandez, A.I., Viron, N., Alhagdow, M., Karimi, M., Jones, M., Amsellem, Z. *et al.* (2009) Flexible tools for gene expression and silencing in tomato. *Plant Physiology*, **151**, 1729–1740. Available from: https://doi.org/10.1104/pp.109.147546

Fonseca, R., Capel, C., Yuste-Lisbona, F.J., Quispe, J.L., Gómez-Martín, C., Lebrón, R. *et al.* (2022) Functional characterization of the tomato HAIR-PLUS gene reveals the implication of the epigenome in the control of glandular trichome formation. *Horticulture Research*, **9**, uhab015. Available from: https://doi.org/10.1093/hr/uhab015

Galdon-Armero, J., Arce-Rodriguez, L., Downie, M., Li, J. & Martin, C. (2020) A scanning electron micrograph-based resource for identification of loci involved in epidermal development in tomato: elucidation of a new function for the Mixta-like transcription factor in leaves. *Plant Cell*, **32**, 1414–1433. Available from: https://doi.org/10.1105/tpc.20.00127

Galindo-González, L., Sarmiento, F. & Quimbaya, M.A. (2018) Shaping plant adaptability, genome structure and gene expression through transposable element epigenetic control: focus on methylation. *Agronomy*, **8**(9), 180. Available from: https://doi.org/10.3390/agronomy8090180

Gao, S., Gao, Y., Xiong, C., Yu, G., Chang, J., Yang, Q. *et al.* (2017) The tomato B-type cyclin gene, SlCycB2, plays key roles in reproductive organ development, trichome initiation, terpenoids biosynthesis and Prodenia litura defense. *Plant Science*, **262**, 103–114. Available from: https://doi.org/10.1016/j.plantsci.2017.05.006

Gehring, M. & Henikoff, S. (2007) DNA methylation dynamics in plant genomes. *Biochim. Biophys. Acta BBA - Gene Struct. Expr.*, **1769**, 276–286. Available from: https://doi.org/10.1016/j.bbaexp.2007.01.009

Gehring, M., **Huh, J.H.**, **Hsieh, T.-F.**, **Penterman, J.**, **Choi, Y.**, **Harada, J.J.** ***et al.*** (2006) DEMETER DNA glycosylase establishes MEDEA Polycomb gene self-imprinting by allele-specific demethylation. *Cell*, **124**, 495–506. Available from: https://doi.org/10.1016/j.cell.2005.12.034

Glas, J., **Schimmel, B.**, **Alba, J.**, **Escobar-Bravo, R.**, **Schuurink, R.** & **Kant, M.** (2012) Plant glandular trichomes as targets for breeding or engineering of resistance to herbivores. *International Journal of Molecular Sciences*, **13**, 17077–17103. Available from: https://doi.org/10.3390/ijms131217077

Gong, Z., **Morales-Ruiz, T.**, **Ariza, R.R.**, **Roldán-Arjona, T.**, **David, L.** & **Zhu, J.-K.** (2002) ROS1, a repressor of transcriptional gene silencing in Arabidopsis, encodes a DNA glycosylase/lyase. *Cell*, **111**, 803–814. Available from: https://doi.org/10.1016/S0092-8674(02)01133-9

Gramzow, L. & **Theissen, G.** (2010) A hitchhiker's guide to the MADS world of plants. *Genome Biology*, **11**, 214. Available from: https://doi.org/10.1186/gb-2010-11-6-214

Grefen, C. & **Harter, K.** (2004) Plant two-component systems: principles, functions, complexity and cross talk. *Planta*, **219**, 733–742. Available from: https://doi.org/10.1007/s00425-004-1316-4

Haeussler, M., **Schönig, K.**, **Eckert, H.**, **Eschstruth, A.**, **Mianné, J.**, **Renaud, J.-B.** ***et al.*** (2016) Evaluation of off-target and on-target scoring algorithms and integration into the guide RNA selection tool CRISPOR. *Genome Biology*, **17**, 148. Available from: https://doi.org/10.1186/s13059-016-1012-2

Harris, C.J., **Scheibe, M.**, **Wongpalee, S.P.**, **Liu, W.**, **Cornett, E.M.**, **Vaughan, R.M.** ***et al.*** (2018) A DNA methylation reader complex that enhances gene transcription. *Science*, **362**, 1182–1186. Available from: https://doi.org/10.1126/science.aar7854

Hollister, J.D. & **Gaut, B.S.** (2009) Epigenetic silencing of transposable elements: a trade-off between reduced transposition and deleterious effects on neighboring gene expression. *Genome Research*, **19**, 1419–1428. Available from: https://doi.org/10.1101/gr.091678.109

Hsieh, T.-F., **Ibarra, C.A.**, **Silva, P.**, **Zemach, A.**, **Eshed-Williams, L.**, **Fischer, R.L.** ***et al.*** (2009) Genome-wide demethylation of Arabidopsis endosperm. *Science*, **324**, 1451–1454. Available from: https://doi.org/10.1126/science.1172417

Hubner, N.C., **Bird, A.W.**, **Cox, J.**, **Splettstoesser, B.**, **Bandilla, P.**, **Poser, I.** ***et al.*** (2010) Quantitative proteomics combined with BAC TransgeneOmics reveals in vivo protein interactions. *The Journal of Cell Biology*, **189**, 739–754. Available from: https://doi.org/10.1083/jcb.200911091

Ibarra, C.A., **Feng, X.**, **Schoft, V.K.**, **Hsieh, T.-F.**, **Uzawa, R.**, **Rodrigues, J.A.** ***et al.*** (2012) Active DNA demethylation in plant companion cells reinforces transposon methylation in gametes. *Science*, **337**, 1360–1364. Available from: https://doi.org/10.1126/science.1224839

Jankovics, F., **Bence, M.**, **Sinka, R.**, **Faragó, A.**, **Bodai, L.**, **Pettkó-Szandtner, A.** ***et al.*** (2018) Drosophila small ovary gene is required for transposon silencing and heterochromatin organization, and ensures germline stem cell maintenance and differentiation. *Development*, **145**(23), dev.170639. Available from: https://doi.org/10.1242/dev.170639

Kertész, S., **Kerényi, Z.**, **Mérai, Z.**, **Bartos, I.**, **Pálfy, T.**, **Barta, E.** ***et al.*** (2006) Both introns and long 3′-UTRs operate as cis-acting elements to trigger nonsense-mediated decay in plants. *Nucleic Acids Research*, **34**, 6147–6157. Available from: https://doi.org/10.1093/nar/gkl737

Kobayashi, K., **Suzuki, T.**, **Iwata, E.**, **Nakamichi, N.**, **Suzuki, T.**, **Chen, P.** ***et al.*** (2015) Transcriptional repression by MYB 3R proteins regulates plant organ growth. *The EMBO Journal*, **34**, 1992–2007. Available from: https://doi.org/10.15252/embj.201490899

Krueger, F. & **Andrews, S.R.** (2011) Bismark: a flexible aligner and methylation caller for bisulfite-seq applications. *Bioinformatics*, **27**, 1571–1572. Available from: https://doi.org/10.1093/bioinformatics/btr167

Lang, Z., **Lei, M.**, **Wang, X.**, **Tang, K.**, **Miki, D.**, **Zhang, H.** ***et al.*** (2015) The methyl-CpG-binding protein MBD7 facilitates active DNA demethylation to limit DNA hyper-methylation and transcriptional gene silencing. *Molecular Cell*, **57**, 971–983. Available from: https://doi.org/10.1016/j.molcel.2015.01.009

Lang, Z., **Wang, Y.**, **Tang, K.**, **Tang, D.**, **Datsenka, T.**, **Cheng, J.** ***et al.*** (2017) Critical roles of DNA demethylation in the activation of ripening-induced genes and inhibition of ripening-repressed genes in tomato fruit. *Proceedings of the National Academy of Sciences*, **114**, E4511–E4519. Available from: https://doi.org/10.1073/pnas.1705233114

Langmead, B. & **Salzberg, S.L.** (2012) Fast gapped-read alignment with bowtie 2. *Nature Methods*, **9**, 357–359. Available from: https://doi.org/10.1038/nmeth.1923

Law, J.A. & **Jacobsen, S.E.** (2010) Establishing, maintaining and modifying DNA methylation patterns in plants and animals. *Nature Reviews. Genetics*, **11**, 204–220. Available from: https://doi.org/10.1038/nrg2719

Lei, M., **Zhang, H.**, **Julian, R.**, **Tang, K.**, **Xie, S.** & **Zhu, J.-K.** (2015) Regulatory link between DNA methylation and active demethylation in Arabidopsis. *Proceedings of the National Academy of Sciences*, **112**, 3553–3557. Available from: https://doi.org/10.1073/pnas.1502279112

Li, Q., **Wang, X.**, **Sun, H.**, **Zeng, J.**, **Cao, Z.**, **Li, Y.** ***et al.*** (2015) Regulation of active DNA demethylation by a methyl-CpG-binding domain protein in Arabidopsis thaliana. *PLoS Genetics*, **11**, e1005210. Available from: https://doi.org/10.1371/journal.pgen.1005210

Li, X., **Harris, C.J.**, **Zhong, Z.**, **Chen, W.**, **Liu, R.**, **Jia, B.** ***et al.*** (2018) Mechanistic insights into plant SUVH family H3K9 methyltransferases and their binding to context-biased non-CG DNA methylation. *Proceedings of the National Academy of Sciences*, **115**, E8793–E8802. Available from: https://doi.org/10.1073/pnas.1809841115

Li, Y., **Deng, H.**, **Miao, M.**, **Li, H.**, **Huang, S.**, **Wang, S.** ***et al.*** (2016) Tomato MBD5, a methyl CpG binding domain protein, physically interacting with UV-damaged DNA binding protein-1, functions in multiple processes. *The New Phytologist*, **210**, 208–226. Available from: https://doi.org/10.1111/nph.13745

Lister, R., **Mukamel, E.A.**, **Nery, J.R.**, **Urich, M.**, **Puddifoot, C.A.**, **Johnson, N.D.** ***et al.*** (2013) Global epigenomic reconfiguration during mammalian brain development. *Science*, **341**, 1237905. Available from: https://doi.org/10.1126/science.1237905

Liu, R., **How-Kit, A.**, **Stammitti, L.**, **Teyssier, E.**, **Rolin, D.**, **Mortain-Bertrand, A.** ***et al.*** (2015) A DEMETER-like DNA demethylase governs tomato fruit ripening. *Proceedings of the National Academy of Sciences*, **112**, 10804–10809. Available from: https://doi.org/10.1073/pnas.1503362112

Liu, R. & **Lang, Z.** (2020) The mechanism and function of active DNA demethylation in plants. *Journal of Integrative Plant Biology*, **62**, 148–159. Available from: https://doi.org/10.1111/jipb.12879

Marone, D., **Russo, M.A.**, **Laidò, G.**, **De Leonardis, A.M.** & **Mastrangelo, A.M.** (2013) Plant nucleotide binding site–leucine-rich repeat (NBS-LRR) genes: active guardians in host defense responses. *International Journal of Molecular Sciences*, **14**, 7302–7326. Available from: https://doi.org/10.3390/ijms14047302

Mason, M.G., **Li, J.**, **Mathews, D.E.**, **Kieber, J.J.** & **Schaller, G.E.** (2004) Type-B response regulators display overlapping expression patterns in Arabidopsis. *Plant Physiology*, **135**, 927–937. Available from: https://doi.org/10.1104/pp.103.038109

Matzke, M.A., **Kanno, T.** & **Matzke, A.J.M.** (2015) RNA-directed DNA methylation: the evolution of a complex epigenetic pathway in flowering plants. *Annual Review of Plant Biology*, **66**, 243–267. Available from: https://doi.org/10.1146/annurev-arplant-043014-114633

Miao, W., **Dai, J.**, **Wang, Y.**, **Wang, Q.**, **Lu, C.**, **La, Y.** ***et al.*** (2021) Roles of IDM3 and SDJ1/2/3 in establishment and/or maintenance of DNA methylation in Arabidopsis. *Plant & Cell Physiology*, **62**, 1409–1422. Available from: https://doi.org/10.1093/pcp/pcab091

Mok, Y.G., **Uzawa, R.**, **Lee, J.**, **Weiner, G.M.**, **Eichman, B.F.**, **Fischer, R.L.** ***et al.*** (2010) Domain structure of the DEMETER 5-methylcytosine DNA glycosylase. *Proceedings of the National Academy of Sciences*, **107**, 19225–19230. Available from: https://doi.org/10.1073/pnas.1014348107

Nie, W.-F., **Lei, M.**, **Zhang, M.**, **Tang, K.**, **Huang, H.**, **Zhang, C.** ***et al.*** (2019) Histone acetylation recruits the SWR1 complex to regulate active DNA demethylation in. *Proceedings of the National Academy of Sciences*, **116** (33), 201906023. Available from: https://doi.org/10.1073/pnas.1906023116

Nyikó, T., **Auber, A.**, **Szabadkai, L.**, **Benkovics, A.**, **Auth, M.**, **Mérai, Z.** ***et al.*** (2017) Expression of the eRF1 translation termination factor is controlled by an autoregulatory circuit involving readthrough and nonsense-mediated decay in plants. *Nucleic Acids Research*, **45**, 4174–4188. Available from: https://doi.org/10.1093/nar/gkw1303

Parida, A.P., **Raghuvanshi, U.**, **Pareek, A.**, **Singh, V.**, **Kumar, R.** & **Sharma, A.K.** (2018) Genome-wide analysis of genes encoding MBD domain-containing proteins from tomato suggest their role in fruit development and abiotic stress responses. *Molecular Biology Reports*, **45**, 2653–2669. Available from: https://doi.org/10.1007/s11033-018-4435-x

Park, Y. & **Wu, H.** (2016) Differential methylation analysis for BS-seq data under general experimental design. *Bioinformatics*, **32**, 1446–1453. Available from: https://doi.org/10.1093/bioinformatics/btw026

Paul, A., **Rao, S.** & **Mathur, S.** (2016) The α-crystallin domain containing genes: identification, phylogeny and expression profiling in abiotic stress, phytohormone response and development in tomato (Solanum lycopersicum). *Frontiers in Plant Science*, **7**, 426. Available from: https://doi.org/10.3389/fpls.2016.00426

Penterman, J., **Zilberman, D.**, **Huh, J.H.**, **Ballinger, T.**, **Henikoff, S.** & **Fischer, R.L.** (2007) DNA demethylation in the Arabidopsis genome. *Proceedings of the National Academy of Sciences*, **104**, 6752–6757. Available from: https://doi.org/10.1073/pnas.0701861104

Pimentel, H., **Bray, N.L.**, **Puente, S.**, **Melsted, P.** & **Pachter, L.** (2017) Differential analysis of RNA-seq incorporating quantification uncertainty. *Nature Methods*, **14**, 687–690. Available from: https://doi.org/10.1038/nmeth.4324

Qian, W., **Miki, D.**, **Lei, M.**, **Zhu, X.**, **Zhang, H.**, **Liu, Y.** ***et al.*** (2014) Regulation of active DNA demethylation by an α-crystallin domain protein in Arabidopsis. *Molecular Cell*, **55**, 361–371. Available from: https://doi.org/10.1016/j.molcel.2014.06.008

Quinlan, A.R. & **Hall, I.M.** (2010) BEDTools: a flexible suite of utilities for comparing genomic features. *Bioinformatics*, **26**, 841–842. Available from: https://doi.org/10.1093/bioinformatics/btq033

Rodríguez-Leal, D., **Lemmon, Z.H.**, **Man, J.**, **Bartlett, M.E.** & **Lippman, Z.B.** (2017) Engineering quantitative trait variation for crop improvement by genome editing. *Cell*, **171**, 470–480. Available from: https://doi.org/10.1016/j.cell.2017.08.030

Schuurink, R. & **Tissier, A.** (2020) Glandular trichomes: micro-organs with model status? *The New Phytologist*, **225**, 2251–2266. Available from: https://doi.org/10.1111/nph.16283

Simmons, A.T. & **Gurr, G.M.** (2005) Trichomes of Lycopersicon species and their hybrids: effects on pests and natural enemies. *Agricultural and Forest Entomology*, **7**, 265–276. Available from: https://doi.org/10.1111/j.1461-9555.2005.00271.x

Tamiru, M., **Hardcastle, T.J.** & **Lewsey, M.G.** (2018) Regulation of genome-wide DNA methylation by mobile small RNAs. *The New Phytologist*, **217**, 540–546. Available from: https://doi.org/10.1111/nph.14874

Tang, K., **Lang, Z.**, **Zhang, H.** & **Zhu, J.-K.** (2016) The DNA demethylase ROS1 targets genomic regions with distinct chromatin modifications. *Nature Plants*, **2**, 1–10. Available from: https://doi.org/10.1038/nplants.2016.169

Wang, J., **Xia, J.**, **Song, Q.**, **Liao, X.**, **Gao, Y.**, **Zheng, F.** ***et al.*** (2020) Genome-wide identification, genomic organization and expression profiles of SlARR-B gene family in tomato. *Journal of Applied Genetics*, **61**, 391–404. Available from: https://doi.org/10.1007/s13353-020-00565-5

Wang, X., **Weigel, D.** & **Smith, L.M.** (2013) Transposon variants and their effects on gene expression in Arabidopsis. *PLoS Genetics*, **9**, e1003255. Available from: https://doi.org/10.1371/journal.pgen.1003255

Werner, S., **Engler, C.**, **Weber, E.**, **Gruetzner, R.** & **Marillonnet, S.** (2012) Fast track assembly of multigene constructs using Golden Gate cloning and the MoClo system. *Bioengineered*, **3**, 38–43. Available from: https://doi.org/10.4161/bbug.3.1.18223

Williams, B.P., **Pignatta, D.**, **Henikoff, S.** & **Gehring, M.** (2015) Methylation-sensitive expression of a DNA demethylase gene serves As an epigenetic rheostat. *PLoS Genetics*, **11**, e1005142. Available from: https://doi.org/10.1371/journal.pgen.1005142

Williams, C.J., **Dai, D.**, **Tran, K.A.**, **Monroe, J.G.** & **Williams, B.P.** (2023) Dynamic DNA methylation turnover in gene bodies is associated with enhanced gene expression plasticity in plants. *Genome Biology*, **24**, 227. Available from: https://doi.org/10.1186/s13059-023-03059-9

Worthen, J.M., **Yamburenko, M.V.**, **Lim, J.**, **Nimchuk, Z.L.**, **Kieber, J.J.** & **Schaller, G.E.** (2019) Type-B response regulators of rice play key roles in growth, development and cytokinin signaling. *Development*, **146**, dev174870. Available from: https://doi.org/10.1242/dev.174870

Wu, H., **Xu, T.**, **Feng, H.**, **Chen, L.**, **Li, B.**, **Yao, B.** ***et al.*** (2015) Detection of differentially methylated regions from whole-genome bisulfite sequencing data without replicates. *Nucleic Acids Research*, **43**, e141. Available from: https://doi.org/10.1093/nar/gkv715

Wu, M., **Chang, J.**, **Han, X.**, **Shen, J.**, **Yang, L.**, **Hu, S.** ***et al.*** (2023) A HD-ZIP transcription factor specifies fates of multicellular trichomes via dosage-dependent mechanisms in tomato. *Developmental Cell*, **58**, 278–288.e5. Available from: https://doi.org/10.1016/j.devcel.2023.01.009

Xiao, X., **Zhang, J.**, **Li, T.**, **Fu, X.**, **Satheesh, V.**, **Niu, Q.** ***et al.*** (2019) A group of SUVH methyl-DNA binding proteins regulate expression of the DNA demethylase ROS1 in Arabidopsis. *Journal of Integrative Plant Biology*, **61**, 110–119. Available from: https://doi.org/10.1111/jipb.12768

Xu, J., **Van Herwijnen, Z.O.**, **Dräger, D.B.**, **Sui, C.**, **Haring, M.A.** & **Schuurink, R.C.** (2018) SlMYC1 regulates type VI glandular trichome formation and terpene biosynthesis in tomato glandular cells. *Plant Cell*, **30**, 2988–3005. Available from: https://doi.org/10.1105/tpc.18.00571

Yamamuro, C., **Miki, D.**, **Zheng, Z.**, **Ma, J.**, **Wang, J.**, **Yang, Z.** ***et al.*** (2014) Overproduction of stomatal lineage cells in Arabidopsis mutants defective in active DNA demethylation. *Nature Communications*, **5**, 4062. Available from: https://doi.org/10.1038/ncomms5062

Yamburenko, M.V., **Worthen, J.M.**, **Zeenat, A.**, **Azhar, B.J.**, **Swain, S.**, **Couitt, A.R.** ***et al.*** (2020) Functional analysis of the Rice type-B response regulator RR22. *Frontiers in Plant Science*, **11**, 577676. Available from: https://doi.org/10.3389/fpls.2020.577676

Yang, C., **Li, H.**, **Zhang, J.**, **Luo, Z.**, **Gong, P.**, **Zhang, C.** ***et al.*** (2011) A regulatory gene induces trichome formation and embryo lethality in tomato. *Proceedings of the National Academy of Sciences*, **108**, 11836–11841. Available from: https://doi.org/10.1073/pnas.1100532108

Zhai, J., **Bischof, S.**, **Wang, H.**, **Feng, S.**, **Lee, T.**, **Teng, C.** ***et al.*** (2015) A one precursor one siRNA model for pol IV-dependent siRNA biogenesis. *Cell*, **163**, 445–455. Available from: https://doi.org/10.1016/j.cell.2015.09.032

Zhang, H., **Gong, Z.** & **Zhu, J.-K.** (2022) Active DNA demethylation in plants: 20 years of discovery and beyond. *Journal of Integrative Plant Biology*, **64**, 2217–2239. Available from: https://doi.org/10.1111/jipb.13423

Zhang, H., **Lang, Z.** & **Zhu, J.-K.** (2018) Dynamics and function of DNA methylation in plants. *Nature Reviews. Molecular Cell Biology*, **19**, 489–506. Available from: https://doi.org/10.1038/s41580-018-0016-z

Zhang, M., **Kimatu, J.N.**, **Xu, K.** & **Liu, B.** (2010) DNA cytosine methylation in plant development. *Journal of Genetics and Genomics*, **37**, 1–12. Available from: https://doi.org/10.1016/S1673-8527(09)60020-5

Zhao, Q.-Q., **Lin, R.-N.**, **Li, L.**, **Chen, S.** & **He, X.-J.** (2019) A methylated-DNA-binding complex required for plant development mediates transcriptional activation of promoter methylated genes: a complex mediates activation of methylated genes. *Journal of Integrative Plant Biology*, **61**, 120–139. Available from: https://doi.org/10.1111/jipb.12767

Zhao, Y., **Xie, S.**, **Li, X.**, **Wang, C.**, **Chen, Z.**, **Lai, J.** ***et al.*** (2014) REPRESSOR OF SILENCING5 encodes a member of the small heat shock protein family and is required for DNA demethylation in Arabidopsis. *Plant Cell*, **26**, 2660–2675. Available from: https://doi.org/10.1105/tpc.114.126730

Zhu, J.-K. (2009) Active DNA demethylation mediated by DNA glycosylases. *Annual Review of Genetics*, **43**, 143–166. Available from: https://doi.org/10.1146/annurev-genet-102108-134205

Zilberman, D., **Coleman-Derr, D.**, **Ballinger, T.** & **Henikoff, S.** (2008) Histone H2A.Z and DNA methylation are mutually antagonistic chromatin marks. *Nature*, **456**, 125–129. Available from: https://doi.org/10.1038/nature07324